JCI insight

Genetic inhibition of serum glucocorticoid kinase 1 prevents obesity-related atrial fibrillation

Aneesh Bapat, … , Saumya Das, David Milan

JCI Insight. 2022. https://doi.org/10.1172/jci.insight.160885.

Research In-Press Preview Cardiology Metabolism

Graphical abstract

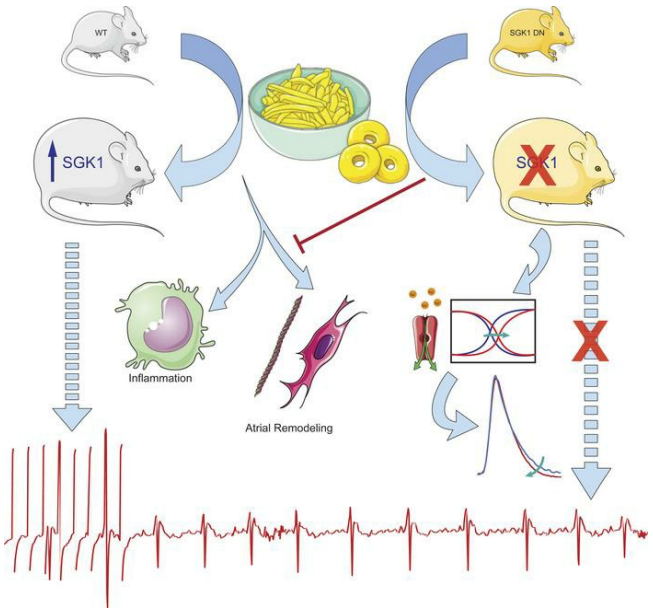

Genetic Inhibition of Serum Glucocorticoid Kinase 1 Prevents Obesity-related Atrial Fibrillation

Running Title: *SGK1 Inhibition for Obesity-related AF*

Aneesh Bapat[1,2], Guoping Li[1], Ling Xiao[1], Ashish Yeri[1], Maarten Hulsmans[3,4], Jana Grune[3-5], Masahiro Yamazoe[3,4], Maximillian J Schloss[3,4], Yoshiko Iwamoto[3,4], Justin Tedeschi[1], Xinyu Yang[6], Matthias Nahrendorf[3,4,7], Anthony Rosenzweig[1], Patrick T. Ellinor[1,2], Saumya Das*[1,2], David Milan*[1,8]

1. Cardiovascular Research Center, Massachusetts General Hospital, Harvard Medical School, Boston, MA, USA.
2. Demoulas Center for Cardiac Arrhythmias, Massachusetts General Hospital, Boston, MA, USA.
3. Center for Systems Biology, Massachusetts General Hospital Research Institute and Harvard Medical School, Boston, MA, USA.
4. Department of Radiology, Massachusetts General Hospital, Boston, MA, USA.
5. German Centre for Cardiovascular Research, Berlin, Germany
6. Fangshan Hospital of Beijing, University of Traditional Chinese Medicine, Beijing, China
7. Department of Internal Medicine I, University Hospital Wuerzburg, Wuerzburg, Germany.
8. Leducq Foundation, Boston, MA, USA

- SD and DM contributed equally to this manuscript and are co-senior authors.

The authors have declared that no conflict of interest exists.

Address Correspondence to:

Saumya Das MD PhD

Cardiovascular Research Center

185 Cambridge Street

Boston, MA 02114.

E: sdas@mgh.harvard.edu

David Milan, MD

265 Franklin St Ste 1902

Boston, MA 02110

E: dmilan@leducq.com

ABSTRACT:

Obesity is an important risk factor for atrial fibrillation (AF), but a better mechanistic understanding of obesity-related atrial fibrillation is required. Serum glucocorticoid kinase 1 (SGK1) is a kinase positioned within multiple obesity-related pathways, and prior work has shown a pathologic role of SGK1 signaling in ventricular arrhythmias. We validated a mouse model of obesity-related AF using wild type mice fed a high fat diet. RNA sequencing of atrial tissue demonstrated substantial differences in gene expression, with enrichment of multiple SGK1-related pathways, and we confirmed upregulated of SGK1 transcription, activation, and signaling in obese atria. Mice expressing a cardiac specific dominant negative SGK1 were protected from obesity-related AF, through effects on atrial electrophysiology, action potential characteristics, structural remodeling, inflammation, and sodium current. Overall, this study demonstrates the promise of targeting SGK1 in a mouse model of obesity-related AF.

INTRODUCTION

The rate of obesity in the US has risen steadily since 1960 and reached a prevalence of 42% in 2017-2018.(1) With a pediatric obesity prevalence of 19% in 2017-2018,(2) we can reasonably expect obesity to persist as a significant public health issue. Atrial fibrillation (AF) is a common cardiac arrhythmia that affects about 5 million Americans and is associated with significant morbidity and mortality.(3) Although many risk factors have been identified for AF, obesity has come to the forefront as a prominent but potentially modifiable one. Epidemiological studies demonstrate that nearly 1 in 5 cases of AF are associated with obesity.(4) Importantly, data from the Women's Health Study showed that obese individuals who lost weight to BMI<30 kg/m^2 over a 5-year follow up period were found to have a reduced AF risk when compared to their persistently obese counterparts.(5) Thus, not only is obesity a strong AF risk factor, but it may be one that is reversible.

The mechanistic relationship between obesity and AF is not completely delineated, and thus no specific therapies exist. However, a plethora of inciting factors have been proposed, and include alterations in hemodynamics, neurohormonal axis, inflammation, metabolism, and adipokines.(6) Animal models of prolonged high fat diet feeding suggest a role for electroanatomic remodeling,(7–10) inflammation,(11) and decreased connexin expression.(12) In addition, obesity is associated with activation of the NLRP3 inflammasome,(13) which can be manipulated in cardiomyocytes to produce an atrial substrate susceptible to AF.(14)

Serum glucocorticoid kinase 1 (SGK1) is a PI3-kinase-dependent kinase, with structure similar to AKT.(15) SGK1 expression and activation lies downstream of both insulin signaling pathways and mineralocorticoid receptor activation(16)- both of which are associated with human AF.(17–24) Additionally, systemic upregulation of both upstream pathways have been noted in multiple models of diet induced obesity,(25–28) positioning SGK1 as a potential key mediator of AF pathogenesis in the context of obesity. Initial studies of SGK1 demonstrated that the signaling pathway can be activated in the heart by transverse aortic constriction, where acute activation promotes cardiomyocyte survival.(29) However, SGK1 was subsequently shown to be activated in human heart failure, pointing to its role in maladaptive cardiac remodeling. Cardiac specific expression of constitutively active SGK1 in mice was associated with worsened TAC-induced cardiac dysfunction and lethal ventricular arrhythmias through electrical remodeling caused by the late sodium current (I_{Na}), while genetic inhibition was protective.(30) SGK1 signaling has also been implicated in murine cardiac inflammation(31) and NLRP3 inflammasome activation(32) resulting from angiotensin II infusion induced hypertension. SGK1 signaling therefore presents a unique and attractive therapeutic target given its presumed involvement in multiple obesity-related pathways, but also its ability to directly modulate cardiac electrophysiology through effects on the sodium current.

Based on its position downstream of metabolic pathways and its known role in electrophysiology, our *a priori* hypothesis was that obesity may induce pathologic SGK1 signaling. We sought to *confirm* our hypothesis with a comprehensive assessment of the effects of obesity on atrial gene expression and found multiple SGK1-related pathways to be upregulated, including insulin and

mineralocorticoid signaling. We then postulated that genetic inhibition of SGK1 would be protective in obesity-related AF through attenuation of obesity-related atrial electroanatomic remodeling and inflammation.

RESULTS

Diet induced obesity results in increased AF susceptibility and marked transcriptional changes

We used diet induced obesity to create a mouse model of obesity-related AF. C57BL/6J wild type (WT) mice were fed a high fat diet (HFD) starting at 6 weeks of age. (Figure 1A) We performed intra-peritoneal glucose tolerance testing (IPGTT) in lean (average weight 30$\pm$2.8 grams) and obese (average weight 42$\pm$3.1 grams) WT mice after 10 weeks of control or HFD. This assessment confirmed a significant difference in glucose tolerance as quantified by area under the curve (AUC), as well as significant differences in blood glucose 15, 60 and 120 minutes after glucose challenge, overall suggesting insulin resistance. (Figure 1B) We then performed terminal EP studies to assay arrhythmogenesis after 4 to 10 weeks of HFD. Although only 1 out of the 6 mice studies was inducible for AF greater than 1 second after 4 weeks of HFD (average weight 31$\pm$2.2 grams), 6 out of 7 were inducible for AF after 10 weeks of HFD. In comparison, among age-matched mice fed a control diet for 10 weeks, only 1 out of 8 was inducible for AF during EP studies. (Figure 1C) Given this stark phenotype at 10 weeks of HFD, we proceeded to use 10 weeks of HFD as a model for obesity-related AF.

In addition to EP studies, a separate group of WT mice were euthanized after 10 weeks of HFD to assess the transcriptional effects of obesity in atrial tissue. RNA sequencing was performed in

atrial tissue of lean and obese wild type C57/Bl6 mice, followed by Gene Set Enrichment Analysis (GSEA) with KEGG pathways to identify affected biological processes. There was marked divergence in the transcriptional profile of lean and obese atria, with 444 differentially expressed genes (279 upregulated, 165 downregulated) between the two groups ($p_{adj}<0.05$). (Supplemental Table 1) All positively and negatively enriched KEGG pathways at a family-wise error rate of <0.05 (FWER p-value) are listed in Supplemental Tables 2 and 3.

Notable among these were KEGG pathways that either directly involve SGK1 signaling, or that lie upstream or downstream of SGK1. Using a broader catchment with a false discovery rate <0.25, we identified 10 SGK1-related KEGG pathways, which are presented in Table 1. Among these, SGK1 is directly involved in "MTOR SIGNALING" and "ALDOSTERONE REGULATED SODIUM ABSORPTION". Beyond this, SGK1 lies downstream of a number of obesity-regulated pathways, including "CHEMOKINE SIGNALING", "INSULIN SIGNALING", and "MAPK SIGNALING". The five SGK1-related pathways with FWER p-value <0.05 are shown in Figure 1D, with differentially expressed (nominal p<0.05) core enriched genes depicted in the heat map. Besides significant upregulation in multiple pathways associated with SGK1 signaling, the RNA sequencing data also suggested an increase in expression of *Sgk1* itself, with a log-2-fold change of 0.285 and a nominal p-value of 0.046. These data supported our hypothesis that obesity-related pathophysiology may overlap with or involve SGK1 signaling. In addition to these findings, the unique role of SGK1 signaling in *ventricular* pro-arrhythmia mediated by electrical remodeling presented it as an opportunistic target for treatment of obesity-related *atrial* arrhythmias.

Diet induced obesity activates SGK1 signaling

The above noted increase in *Sgk1* gene expression was confirmed with focused quantitative PCR, as HFD resulted in a significant increase in atrial SGK1 gene expression, with a similar trend in the ventricles. (Figure 1E-F) In addition, in both atrial and ventricular tissue, high fat diet feeding led to a significant increase in the ratio of phosphorylated to total SGK1 as determined by Western blotting. (Figure 1E-F) In order to further ascertain SGK1 signaling we quantified phosphorylation of known SGK1 targets. In fact, there was a marked increase in phosphorylation of SGK1-specific target NDRG1 in both obese atrial and ventricular tissue. Similarly, in obese atrial tissue, there was an increase in phosphorylated GSK3β; there was no difference in GSK3β in ventricular tissue. (Figure 1G,H) Overall, these data demonstrate that diet induced obesity resulted both in increased AF inducibility, as well as an increase in SGK1 transcription, SGK1 activation through phosphorylation, and activity assayed by phosphorylation of known SGK1 targets. (Figure 1I) Interestingly, these findings appear more pronounced in atrial, rather than ventricular, tissue. We then investigated the possibility of a dose response relating HFD/obesity with atrial SGK1 signaling, by comparing mice fed HFD for 6 weeks (which have ~50% AF inducibility) with mice fed HFD for 10 weeks. As would be expected, we found an increase in SGK1 and downstream target phosphorylation in mice fed HFD for 10 weeks as compared their counterparts fed for only 6 weeks. (Supplemental Figure 1) Given the known role of SGK1 in electrical/structural remodeling, we sought to investigate the role of SGK1 in obesity-induced atrial pathology.

Genetic SGK1 inhibition alters atrial electrophysiology and prevents obesity-related AF

In order to test whether SGK1 plays a role in obesity-induced AF we employed a previously described transgenic mouse model that overexpresses a dominant negative form of SGK1 in cardiomyocytes (SGK1 DN).(30) After 10-14 weeks of high fat diet, 79% of SGK1 DN (23 out of 29) and 73% of WT littermates (22 out of 30) achieved a minimum 34g weight. (Figure 1A) Over the course of feeding, there were no differences in weight gain or the final weight between SGK1 DN and WT littermates; both were significantly heavier than the WT mice fed a normal chow at the end of the feeding period ($p<5E-5$ for both). Tail cuff blood pressure measurements showed no difference in systolic, diastolic, or mean arterial pressure between the lean WT, obese WT, or obese SGK1 DN mice. Two-dimensional transthoracic echocardiography (TTE) was performed and did not reveal any differences in LV dimensions, LV systolic or diastolic function, or left atrial size between the three groups of mice. Both obese WT and obese SGK1 DN mice demonstrated impaired glucose tolerance as compared to lean WT mice, but there were no significant differences between the two obese groups. (Supplemental Figure 2) Importantly, assessment of downstream phosphorylation targets in SGK1 DN atria confirmed a significant decrease in the phosphorylation of NDRG1, and a trend towards the same with respect to GSK3β. (Supplemental Figure 3)

Ambulatory telemetry was performed in obese SGK1 DN and WT mice. Eight-hour periods (from midnight to 8AM) were analyzed to assess for baseline characteristics as well as spontaneous arrhythmias. There were no significant differences in baseline ambulatory HR or the root mean square of the successive differences, (RMSSD) a marker of heart rate variability, between the two groups. (Supplemental Figure 2) No sustained spontaneous arrhythmias (atrial or ventricular)

were recorded during the analyzed periods. However, there was a difference in the number of premature atrial complexes (PACs), which was significantly higher in the obese WT group as compared to the obese SGK1 DN group. (Figure 2B). The latter is suggestive of an increased atrial excitability that may serve to trigger AF.

Terminal EP studies were performed to determine EP parameters with focus on AF inducibility. Parameters related to sinus node function, AV node function, and refractory periods in atria and ventricles are presented in Table 2. There were no significant differences in baseline parameters among the three groups. Programmed electrical stimulation with up to 2 extra-stimuli and rapid burst pacing were performed in both the atria and ventricles. AF inducibility was significantly higher in obese (9 out of 9) versus lean mice (0 out of 3), but this difference was abrogated in obese SGK1 DN mice (2 out of 9). There were similar differences in number of AF episodes (>250ms) and total AF burden between lean and obese WT mice which were prevented by SGK1 genetic inhibition. (Figure 2C-D)

Optical mapping of right atrial and left atrial appendages was performed on these three groups of mice using a voltage sensitive dye. (Table 3) There were no significant differences in lean versus obese WT mouse action potential duration, conduction velocity, or AP upstroke velocity in either atrial chamber. Overall, the action potential duration was generally shorter in the obese SGK1 DN as compared to the obese WT mice in both atrial chambers and met statistical significance at 90% repolarization (APD90). (Figure 3A) There were no significant differences in conduction velocity (CV) between the two obese mouse genotypes. Interestingly, within the WT obese mice,

there were significant inter-atrial differences in APD50, CV and dV/dt; lean WT mice had no significant analogous inter-atrial differences, and SGK1 DN mice only had inter-atrial differences in CV, with no significant inter-atrial differences in APDs or dV/dt. (Figure 3B) In order to interrogate this further, we assessed expression and phosphorylation status of SGK1 protein in right and left atria of lean and obese mice (Figure 3C). Pair-wise comparisons revealed generally higher SGK1 phosphorylation in right- versus left- atria, but this difference was exaggerated and met statistical significance in the obese mice.

We performed focused patch clamping on atrial myocytes to further investigate the shorter APDs in setting of SGK1 inhibition. Adipokines such as leptin have been shown to increase the late sodium current in left atrial myocytes.(33) Prior work has demonstrated the effect of SGK1 activation on sodium current via alteration of channel biophysical properties, as well as trafficking and localization of $Na_V1.5$, the pore forming subunit of the channel.(30) We suspected that the protective electrophysiologic consequences of SGK1 genetic inhibition may result from its effects on the sodium current. Whole cell patch clamp was performed on obese WT and obese SGK1 DN left atrial myocytes. (Figure 4A) There were no significant differences in peak I_{Na} between the two groups (Figure 4B) However, SGK1 DN myocytes demonstrated a rightward depolarizing shift in activation-inactivation kinetics of I_{Na} in SGK1 DN myocytes (Inactivation $V_{1/2} \pm$ SEM: WT, -84$\pm$2 mV, N=10, SGK1 DN, -77$\pm$2 mV, N=11, $p<0.05$ WT versus DN). However there were no significant differences in slope factors (mean $\pm$ SEM: WT 0.3$\pm$0.1, SGK1 DN 0.4$\pm$0.1, p=0.62) or activation $V_{1/2}$ (mean $\pm$ SEM: WT -75$\pm$-2.3 mV, SGK1 DN -70.75$\pm$1.8 mV, p=0.145). (Figure 4C) This change in the activation-inactivation curves is diametrically opposed to existing literature on SGK1 CA

cardiomyocytes, which have a *leftward* shift in activation-inactivation kinetics as compared to wild type cells.(30) The rightward shift in activation-inactivation kinetics observed in our study would be expected to decrease the persistent (late) Na current.(34) As the effects of SGK1 signaling on sodium current are mediated by post-translational modification and trafficking, there were unsurprisingly no differences in expression of the $Na_V1.5$ protein subunit as assessed by Western blotting in lean WT, obese WT, or obese SGK1 DN mouse atria. (Figure 4D) These data are consistent with previously published data regarding the effect of SGK1 signaling on I_{Na} in ventricular myocytes(30) and may account for the differences between obese WT and SGK1 DN mouse atria determined through optical mapping. In addition, these data suggest that inter-atrial differences in activation of SGK1 (via phosphorylation) may contribute to the correlating differences in electrophysiology, particularly APD, between the two atrial chambers.

Genetic inhibition of SGK1 prevents cardiac remodeling

SGK1 DN mouse ventricles are resistant to TAC-induced fibrosis,(30) so we hypothesized that SGK1 inhibition may protect from obesity-induced structural remodeling in the atria. We initially performed Masson-Trichrome staining to assess for obesity-related atrial fibrosis. Although obesity-induced atrial fibrosis is described in literature, (35, 36) this is an insensitive technique susceptible to sampling bias, and we did not, in fact, find a difference in fibrosis. (Supplemental Figure 4) However, given the relatively short duration of HFD, we suspected that genetic expression may better reflect the early pro-fibrotic consequences of obesity. Given the association between both atrial and ventricular fibrosis and atrial fibrillation, RT-qPCR of fibrosis-related genes was performed in both tissues. There seemed to be a generalized obesity-induced

increase in pro-fibrotic gene expression in the ventricles, but no significant obesity-induced differences in atrial tissue. However, SGK1 inhibition did result in generally decreased expression of these pro-fibrotic genes in both atria and ventricles (Figure 5A). Activity – and ratio- of matrix metalloproteinases (MMP) and tissue inhibitors of matrix metalloproteinases (TIMP) is known to affect the maintenance and turnover of the extra-cellular matrix (ECM).(37–39) High fat diet feeding was associated with a significantly increased atrial/ventricular expression of tissue inhibitor of metalloproteinase 1 (*Timp1*) and plasminogen activator inhibitor 1 (*Pai-1*), both of which are associated with increased ECM turnover. These obesity-induced pro-fibrotic changes were significantly reduced in ventricular – but not atrial- tissue of SGK1 DN mice. However, the ratios of *Timp1/Mmp2* and *Timp1/Mmp9* were increased in obese WT atria/ventricles as compared to lean WT mouse atria/ventricles, but these ratios were significantly lower in the obese SGK1 DN mice as compared to obese WT mice. (Figure 5A). In addition to differences in gene transcription, Western blotting revealed a significant decrease in atrial protein expression of connective tissue growth factor (CTGF) in SGK1 DN as compared to WT obese mouse atria. (Figure 5B) Overall, these data demonstrate decreased profibrotic signaling in SGK1 DN cardiac tissue even in the relatively short time-period studied, consistent with the previously described finding of reduced ventricular fibrosis in the TAC model.

Multiple animal models have demonstrated the obesity related downregulation of cardiac connexin proteins.(11, 12) We confirmed these results in our study by determining the level of gene and protein expression. Quantitative PCR showed a decrease in atrial expression of both connexin 40 and 43 in obese as compared to lean mice, but the decrease was mitigated or

reversed by SGK1 inhibition. These findings extended to protein translation, as immunoblotting revealed obesity- related decrease in atrial protein expression of connexin 40 and 43 which were ameliorated with SGK1 inhibition. (Figure 5C-D) The data presented here suggest a protective effect of SGK1 inhibition in terms of pro-fibrotic signaling and cell-cell connectivity.

Genetic inhibition of SGK1 prevents obesity- induced inflammation

Inflammation is thought to be involved in obesity induced pathology (including fibrosis),(40) and we suspected that SGK1 signaling may contribute to pro-inflammatory pathways in the heart. We therefore evaluated the effect of SGK1 inhibition on atrial inflammation caused by obesity with quantitative RT-PCR of inflammatory genes in WT lean, WT obese, and SGK1 DN obese mice. The genes of interest were either cytokines known to be involved in obesity-related inflammation or those thought to lie downstream of either mineralocorticoid or SGK1 signaling.(32, 41–44) Once again, cardiomyocyte specific genetic inhibition of SGK1 minimized obesity induced increases in genes related to inflammation. (Figure 6A) Given that SGK1 inhibition is restricted to cardiomyocytes, it is not surprising that plasma levels of circulating cytokines such as IL-6 and CRP were not impacted. (Supplemental Figure 5)

Of note, there was a marked obesity-induced atrial *Il-1β* expression, which was abolished with genetic inhibition of SGK1. SGK1 activation has been shown to affect expression of chemokine ligand 2 (*Ccl2*), which is involved in the recruitment of inflammatory cells such as macrophages.(41) Our data demonstrated a trend towards an increase in obesity-induced *Ccl2* expression, which was prevented by SGK1 genetic inhibition (ANOVA p=0.05). We interrogated

this pathway further with flow cytometry and determined that SGK1 genetic inhibition abrogated a trend towards an increased atrial macrophage content caused by obesity. (Figure 6B) Although one could presume sheer difference in quantity of inflammatory cells as the source of the increase in *Il-1β*, we pursued this avenue further by investigating downstream pathways.

We studied two inter-related pathways that we suspected may have been inhibited with SGK1 inhibition: the NLRP3 inflammasome and NFκB signaling. The NLRP3 inflammasome has been implicated in various obesity-related pathologies, including AF, and has been shown to be inhibited by pharmacologic SGK1 inhibition.(32) Additionally, SGK1 activity has been shown to provoke nuclear translocation and hence activation of nuclear factor κB.(45–47) We assayed inflammasome activity with a fluorometric measurement of caspase activity, which was found to be significantly lower in atrial tissue of SGK1 DN mice compared to WT. (Figure 6C) Similar to *Nlrp3* gene expression, NLRP3 protein expression showed a trend towards an increase with HFD feeding which was significantly reduced with genetic SGK1 inhibition. There were not, however, differences in caspase-1 protein expression (Figure 6D). Finally, EP studies were performed in age-matched obese NLRP3$^{-/-}$ mice which demonstrated an intermediate AF phenotype, with 4 out of 10 mice inducible for AF greater than one second in duration. (Supplemental Table 4)

NLRP3 expression is closely linked to NFκB activation, which is mechanistically downstream of SGK1 activation.(48, 49) Western blotting of the p65 subunit of NFκB revealed an obesity-related significant increase in the phosphorylated – and hence transactivated (50, 51) - form of the protein, which was reversed by SGK1 genetic inhibition. Although there was no significant

difference in the total expression of NFkB p65 between WT lean and obese mice, there was significantly less NFkB p65 protein expression in obese SGK1 DN mouse atria as compared to WT counterparts. (Figure 6E) Overall, these data suggest that the protective effect of SGK1 inhibition in *Il-1β* expression may be mediated in part, by its role in modulating the NLRP3 and NFκB pathways.

Constitutive SGK1 activation may modulate AF susceptibility in HFD-induced obesity

To determine whether SGK1 overactivation on its own affects AF susceptibility, we performed EP studies and optical mapping on age-matched lean SGK1 CA and WT mice. There were no differences in AF inducibility noted between the two groups. Interestingly, SGK1 CA mice demonstrated a significantly longer PR interval, and had a trend (p=0.14) towards a longer Wenckebach cycle length than their WT counterparts, suggesting an effect on AV node function. Otherwise, there were no other significant differences in EP parameters between the two lean groups. (Supplemental Table 5) Optical mapping of lean SGK1 CA mouse hearts reproduced the inter-atrial heterogeneity seen with obese WT mice, as the RA APD50 was significantly longer than LA APD50; there was no correlating inter-atrial difference in lean WT mouse atria. (Figure 7B) In addition, SGK1 CA mice demonstrated a significant increase in RA CV, APDs (50%, 70%, and 90%), and dV/dt as compared to WT mouse atria. (Figure 7C, Supplemental Table 6)

In order to further interrogate SGK1 overactivation, we then utilized the HFD mouse model again. In this case, we fed WT and SGK1 CA mice a HFD for 6 weeks, and then proceeded with basic characterization as well as electrophysiologic and biochemical studies. (Supplemental Figure 6)

Again, telemetry was done and 8-hour periods (midnight to 8AM) were analyzed in WT and SGK1 CA mice. Although there were no spontaneous sustained arrhythmias in either group, there were significantly more PACs in the SGK1 CA mice as compared to the WT mice, again suggesting a role for SGK1 signaling in atrial electrical excitability. (Figure 7E) During invasive EP studies, SGK1 CA mice demonstrated slowed AV nodal conduction, with a significantly longer Wenckebach cycle length and PR interval. (Supplemental Table 7) Although there was no difference in the proportion of mice inducible for AF > 1s, there was a significant increase in the number of inducible AF episodes in the SGK1 CA mice as compared to their WT counterparts and a similar trend was seen in AF burden. (Figure 7E) In order to better assess the general mechanism of arrhythmogenesis, optical mapping was performed on these two groups of mice. SGK1 CA left and right atria demonstrated an overall increase in APD as compared to the WT mouse atria, which met statistical significance at 70% and 90% repolarization. (Figure 7F). Interestingly, conduction velocity was also generally higher in SGK1 CA mice as compared to WT mice, and this difference met statistical significance in the left atrium. (Supplemental Table 8) Finally, qRT-PCR was done in these WT and SGK1 CA atria and revealed a significant increase in *Col1A1* and *Nlrp3* transcripts in CA mouse atria. (Figure 7G) Together our data suggest opposing effects of SGK1 activity on obesity-related AF, with SGK1 activation promoting development of AF coincident with increased fibrosis and inflammation, while SGK1 inhibition was protective against these pathologic changes.

DISCUSSION

Obesity is a reversible risk factor for AF, and the rate of obesity continues unabated at epidemic proportions. Prior work examining the link between obesity and AF has implicated fibrosis, connexin dysregulation, inflammation and ion channel alterations in arrhythmogenesis. Here, we demonstrate marked alteration in atrial gene expression brought on by obesity and an obesity-induced upregulation of atrial SGK1 transcription, activation, and activity. SGK1 inhibition is associated with a reduction in spontaneous atrial ectopy as well as AF inducibility in a mouse model of high fat diet induced obesity. This protective effect was associated with alterations in atrial electrophysiology as well as an attenuation in the obesity-related structural remodeling and inflammation. Overall, SGK1 inhibition prevents some of the pathologic effects of obesity, making it a necessary signaling pathway and an attractive therapeutic target in this AF model. We posit that SGK1 likely interacts with other obesity-related adverse signaling pathways, and that inhibiting SGK1 can therefore mitigate the development of AF.

Despite the established role of obesity in cardiovascular disease, there is limited data regarding the transcriptional effects of obesity on the heart. In a similar mouse model, existing literature has shown that obesity-induced transcriptional changes in the left ventricle largely affect genes and pathways involved in cardiac metabolism including glycolysis as well as remodeling.(52) Here we present the effects of obesity on *atrial* gene expression, which seems to largely affect genes involved in cardiac metabolism, cell-cell connectivity, cardiac remodeling, and cytokine signaling. Importantly, the sequencing data presented here confirmed our pre-existing hypothesis that obesity may result in activation of SGK1-related pathways, and we demonstrated increased insulin signaling, mineralocorticoid signaling, and mTOR signaling.

While cardiac SGK1 activity may be protective in acute pressure overload,(29) persistent activation during chronic pressure overload has been shown to be maladaptive.(30) In models of metabolic syndrome, SGK1 signaling in hepatocytes(53) and adipocytes(54) has been shown to exacerbate insulin resistance. SGK1 is transcriptionally upregulated by circulating factors including glucocorticoids, mineralocorticoids, and insulin.(55) Given the latter, we suspected that obese mice, which are known to have glucose intolerance,(56) may have increased SGK1 expression. We demonstrate here that in fact diet induced obesity does increase both atrial and ventricular SGK1 transcription and signaling. This is a novel finding in the heart, but is an extension of existing literature, which demonstrates obesity-related increases in SGK1 signaling in the aorta,(25) adipose tissue,(26) and in the hippocampus.(27)

From a macroscopic electrophysiologic perspective, we found a marked difference in inducibility of atrial arrhythmias in lean and obese mice. Despite this phenotype, there did not seem to be proportionate differences in surrogate EP parameters, including measures of tissue refractoriness and optical electrophysiologic parameters. We did find, however, inter-atrial differences in action potential characteristics and impulse propagation that were brought on by obesity but reversed with SGK1 inhibition. While this finding may contribute to AF phenotype, it is not independently sufficient to drive AF, as lean SGK1 CA mice – which develop these inter-atrial differences- are not inducible for AF. Further investigation will be necessary to determine the role of SGK1 signaling in defining atrial “sidedness”.

Obesity has been implicated in the development of both the triggers and substrate that underlie cardiac arrhythmias.(6) There is discordant data regarding the effect of obesity on the cardiac sodium current(33, 57–60) and both gain of function(61) and loss of function(62) mutations in the *SCN5a* gene have been associated with AF in families. A particularly relevant recent study of mice with diet-induced obesity, for example, demonstrated decreased expression of the sodium channel subunit $Na_V1.5$ associated with a decrease in I_{Na} as well as APD shortening and decreased dV/dt_{max} in obese- as compared to lean- mouse left atria.(35) These data would seem to stand in contrast to our findings, as we did not find an obesity-related reduction in $Na_V1.5$ expression. However, despite the apparent contradiction, the same mouse model had 25% reduction in AF burden when treated with flecainide, an I_{Na} blocker.(63) A recent study confirmed the pro-AF potential of excess I_{Na}, as it was shown to lead to atrial myopathy, remodeling, and arrhythmia.(64) We did not specifically study the effects of obesity on atrial I_{Na} (as compared to lean mice), but found that the protective effect of SGK1 inhibition in obese mice was associated with a depolarizing shift in the 'window' current for I_{Na} in the atria; this may be expected to decrease late I_{Na}.(34) This finding is consistent with prior literature showing a leftward hyperpolarizing shift in the "window" current as the mechanism for pro-arrhythmia in *constitutive* SGK1 activation.(30) In the context of available literature, our results suggest that I_{Na} regulation may be protective in obesity-related AF, but this only partially explains the benefit derived from SGK1 genetic inhibition.

There is substantial data suggesting a role for obesity-induced structural remodeling in the pathogenesis of atrial fibrillation. Proposed mechanisms include interstitial fibrosis,(7, 8, 10)

connexin dysregulation,(11, 12) and even fatty infiltration.(7) SGK1 activity in particular is associated with a number of fibrosing conditions throughout the body and may be stimulated by TGF-β activity.(65) Here we demonstrate the protective effect of SGK1 inhibition in the expression of several pro-fibrotic factors, including collagen, CTGF and α-SMA. Since we do not find a significant difference in histologic fibrosis, it is possible that the transcriptional/translational changes are a more sensitive assay or may be early signs of fibrosis, but we cannot draw any firm conclusions.(66) MMPs and TIMPs have generally antagonistic functions and work in concert to maintain the homeostatic balance of the extracellular matrix.(37, 38) The relative changes seen here with obesity- which mimic those seen in aged, frail mouse atria-(39) may suggest a profibrotic transcriptional programming. Finally, the role of SGK1 signaling on cardiomyocyte connexin expression are not described in literature, but there is extensive data regarding the effects of fibrosis and inflammation on connexin expression. Our data is consistent with a secondary effect of fibrosis and inflammation on connexin expression, rather than a primary effect of SGK1 regulation.

The protective effects of SGK1 genetic inhibition are consistent with data examining the effects of cardiomyocyte mineralocorticoid receptor knockout.(67) Despite the protective effects of SGK1 inhibition on atrial and ventricular fibrotic signaling, detailed echocardiographic assessment of systolic and diastolic function did not reveal any notable effects of obesity or SGK1 inhibition. Thus, importantly, the protective effect of SGK1 inhibition on AF inducibility in this model is unlikely to derive from hemodynamic effects or effects on LA pressure secondary to the

beneficial effects of SGK1 on ventricular remodeling, but rather suggest a primary beneficial effect of SGK1 inhibition on AF pathogenesis.

SGK1 activation has been linked to inflammation via both the NLRP3 inflammasome as well as NF-κB signaling. With respect to the latter, SGK1 directly phosphorylates IKKα, resulting in increased NF-κB activity.(49) SGK1 dependent NF-κB activation has been demonstrated in renal collecting ducts(68) and aortic vascular smooth muscle cells.(69) Recent literature has posited cardiomyocyte NLRP3 overexpression as a sufficient trigger for AF,(14) and our data regarding atrial NLRP3 expression is compelling in this context. Prior studies have demonstrated an association between SGK1 and inflammasome activity, but the exact mechanism has not been clearly delineated. In a model of hypoxia-induced pulmonary arterial hypertension, SGK1 activity was shown to be associated with hypoxic pulmonary macrophage infiltration, whereby knockout of SGK1 reduced macrophage content.(70) Meanwhile, a specific SGK1 inhibitor was shown to reduce NLRP3 inflammasome expression and mitigate angiotensin II induced cardiac inflammation and fibrosis.(32) In our model, obesity resulted in a marked elevation in IL-1β- a cytokine frequently cited as pro-arrhythmic- which was prevented by SGK1 inhibition, perhaps through its effects on the NF-κB and NLRP3 axes.

An interesting aspect of this study to take note of – as in the *Das et al*(30) study regarding TAC-induced cardiac remodeling- is that our model of SGK1 knockdown is restricted to cardiomyocytes via the αMHC promoter. Yet, the effects seemingly extend to functions classically thought to be driven by non-cardiomyocytes; ECM maintenance is generally attributed to

activated fibroblasts, and inflammation to monocytes. However, *in vitro,* cardiomyocytes have been shown to be capable of expressing fibrosis related transcripts,(71) and even do so in response to leptin exposure.(72) Murine *in vivo* models of cardiac fibrosis due to pressure overload have demonstrated an essential role for cardiomyocyte-dependent TGF-β signaling.(73) There is limited data regarding the role of cardiomyocyte derived signaling in inflammation, but cardiomyocyte calmodulin kinase - through both NLRP3 and NF-κB – is essential to pressure overload induced cardiac inflammation.(74, 75) A particularly relevant study from *Rickard et al*(67) demonstrated cardiomyocyte mineralocorticoid receptors as essential in mineralocorticoid and salt induced cardiac fibrosis and inflammation. This is of critical interest in the context of our data, as the SGK1 axis lies downstream of mineralocorticoid receptor signaling via transcriptional regulation.

We acknowledge several limitations in our study. While bulk RNA sequencing is valuable in identifying perturbed pathways through differences in gene expression, it does not account for the complex cellular composition of cardiac tissue and the changes herein that ultimately affect gene expression. Future experiments assessing transcription at the single cell level in the heart of obese animals may yield interesting information on the role of different cardiac cells in mediating AF pathogenesis. Human obesity is often associated with hypertension and hypertensive heart disease, but we did not find any evidence of either with tail-cuff BP and with echocardiographic assessment of BP. We concede that these approaches have their limitations, and may not be as sensitive as cardiac MRI, strain imaging, and/or invasive radio telemetry.(76, 77) However, we suspect that the short duration of high fat diet feeding may not result in

increased afterload, and that the cardiomyocyte-specificity of SGK1 knockdown would minimize any possible confounding effects of hypertension or vascular resistance in our study. At first glance, it would seem that the stark differences in AF inducibility caused by SGK1 inhibition are incompletely explained by the less pronounced mechanistic differences. We propose that SGK1 inhibition- through its pleiotropic effects- decreases AF susceptibility via multiple contributory mechanisms. Another limitation innate to any rodent studies of AF is that a "positive" finding typically represents very brief (on the order of seconds) episodes of atrial tachyarrhythmia that are induced *in vivo*; i.e., these episodes are neither spontaneous nor sustained. We would argue that mouse models of AF are reasonable models of the substrate, with the trigger provided by pacing/stimulation. Finally, pharmacological inhibition of endogenous SGK1 in this model would have provided complementary data to augment our hypothesis that SGK1 inhibition may be a novel approach to obesity-related AF, but poor bioavailability, potency, and specificity of commercially available SGK1 inhibitors currently limit their utility.

In summary, this study suggests that targeting of SGK1 should be further investigated for its therapeutic potential in obesity-related AF. Through bulk RNA sequencing, we reveal the marked effects of obesity on the atrial transcriptome and describe a number of paths that may lead from obesity to AF beyond ion channel alterations. Notably, SGK1 activity seems to be required for many of these pro-arrhythmic pathways, suggesting a central role for this kinase in obesity-related AF, and thus making inhibition a potentially attractive target for intervention. Future work will include assessing the role of SGK1 inhibition in other AF-related stressors known to activate SGK1 signaling, such as hypertension, and assessment of pharmacologic SGK1 inhibition.

METHODS

The **Supplemental Methods** section includes detailed descriptions of the following procedures/techniques: transthoracic echocardiography, tail-cuff blood pressure, intra-peritoneal glucose tolerance testing, immunoblotting, flow cytometry, histology and fibrosis quantification, and cytokine ELISAs. The RNA sequencing data have been uploaded to the Gene Expression Omnibus (GEO) database with free accessibility (GSE211229).

Animal Studies

SGK1 dominant negative (DN) and constitutively active (CA) mice were generated as previously described, with cardiac-specific expression of a constitutively active (S422D) or dominant negative (K127M) SGK1 transgene driven by the α-myosin heavy chain promotor.(30) Cardiac specificity was confirmed by immunoblotting for an incorporated hemagglutinin (HA) epitope tag. (Supplemental Figure 7A) Transgene carrying mice were bred with wild type C57BL/6J mice to generate litters of transgenic and WT mice. Mice were genotyped by PCR for the presence of the transgene using tail DNA and the following primers: forward 5'-GGTAGCAATCCTCATCGCTTTC-3', reverse 5'-CTTCAGGGTGTTTGCATGCA-3'. (Supplemental Figure 7B) Starting at 6 weeks of age, the SGK1 DN and WT littermates were fed a high fat diet (Research Diets D12492, 60% fat by calories) for at least 10 weeks and up to 14 weeks until body weight was at least 34g. The weight cut-off was approximately the 95th weight percentile among mice fed a control diet and was used to exclude mice that may be resistant to diet induced obesity.(78) Lean mice were fed a standard control chow. Electrophysiology (EP) studies were performed

under general anesthesia and terminated with extraction of the heart. Optical mapping and biochemical analyses required heart extraction, which was performed under deep anesthesia.

Transthoracic Echocardiography

Transthoracic echocardiograms were performed in anesthetized mice using a Vevo® 3100 high-resolution Imaging System coupled to a MX250s ultra-high frequency linear array transducer (15-30 MHz, center transmit: 21 MHz, axial resolution: 75 µm) (both FUJIFILM VisualSonics, Toronto, Ontario, Canada) as described previously.(79, 80) A detailed description is available in the supplemental methods section.

Electrophysiology Studies

EP studies were performed under general anesthesia induced by administering 5% isoflurane driven by an oxygen source into an induction chamber. Anesthesia was subsequently maintained with 1%–2% isoflurane in 95% O_2. A warming blanket was used to maintain a rectal temperature of 35-37^o Celsius to avoid hypothermia. An octapolar catheter (EPR-800, Millar) was inserted into the right jugular vein and positioned in the right atrium and ventricle; the position was ascertained with continuous monitoring of the intracardiac electrograms. Sinus node function was determined by measuring the sinus node recovery time (SNRT) following 30 seconds of pacing at three cycle lengths (120, 100 and 80 ms). The Wenckebach cycle length was determined with progressively faster atrial pacing rates. Atrial, ventricular, and AV nodal refractory periods were measured using programmed electrical stimulation with overdrive pacing trains at 100ms followed by single extra-stimuli. Retrograde (VA) conduction Wenckebach cycle length was

measured by pacing at progressively faster ventricular pacing rates. Provocative testing for arrhythmia induction was performed with double extra-stimuli (S1-S2-S3) at two S1 cycle lengths (120 and 100ms) and progressively decreasing S2 and S3 to 10ms. Additionally, rapid burst pacing was performed at gradually faster rates (starting at 50ms) to a pacing cycle length of 20ms and lasting 3s and 6s. Atrial fibrillation (AF) was defined as a rapid atrial rhythm with atrial rate greater than ventricular rate and irregular ventricular response (R-R intervals). The duration of AF was measured from the end of the pacing train to the end of the rapid atrial activity. Mice were considered *inducible* if they had at least one episodes of AF >1s in duration.

Telemetry

Continuous ambulatory monitoring in obese WT and SGK1 DN mice was achieved with implanted wireless telemetry devices (ETA-F10 transmitter, Data Sciences International, MN, USA) as previously described.(81) Under general anesthesia, telemetry devices were implanted into the abdominal cavity and electrodes were tunneled to a modified lead II position. Telemetry recordings were performed continuously for three months. Data analysis was performed using LabChart 8 (AD Instruments, Colorado Springs, CO).

Optical Mapping

Isolation and perfusion of the heart was performed as previously described.(82, 83) Briefly, the mouse was anaesthetized using isoflurane, the heart excised, and perfused via an aortic cannula. The cannulated heart was perfused with a modified Tyrode solution (128.2 mM NaCl, 4.7 mM KCl, 1.19 mM NaH_2PO4, 1.05 mM $MgCl_2$, 1.3 mM $CaCl_2$, 20.0 mM $NaHCO_3$, 11.1 mM

glucose; pH 7.35±0.05) using a Langendorff perfusion setup. Blebbistatin (10 mM, Tocris Bioscience) was used to arrest cardiac motion. The heart was stained for 30 min with a voltage sensitive dye (di-4-ANEPPs, 2 mmol/L in Dimethyl sulfoxide). Custom-made epicardial platinum electrodes and a Medtronic stimulator were used to pace the heart. Pacing was performed at 60-120ms cycle lengths at twice the capture threshold (4 ms square wave stimuli). A halogen light source (X-Cite 150W, filtered at 520+45 nm) was used to excite fluorescence. Emissions >610 nm were collected and focused onto an 80 × 80 CCD camera (RedShirt Imaging SMQ Camera and Macroscope IIA) using a 50 mm ×2.7 lens (numerical aperture 0.4). Data sampling was performed at 2000 frames per second with a filter setting of 1 kHz. A specifically designed Matlab program was used to perform data analysis in order to generate conduction velocities and APD at 50, 70, and 90% repolarization.

Cardiomyocyte Isolation

Mice were anaesthetized as described above and injected intraperitoneally with 0.2 cc heparin. Hearts were then dissected and mounted on a Langendorff system (Radnoti) via aortic cannulation. Hearts were perfused with Ca^{2+}-free normal Tyrode's solution containing NaCl 137 mM, KCl 4 mM, $MgCl_2$ 1mM, HEPES 10 mM, NaH_2PO_4 0.33 mM, taurine 5mM and dextrose 10 mM (pH 7.4), followed by the same perfusion buffer containing collagenase D and B (0.48 mg/ml and 0.36 mg/ml, respectively; Roche) and protease XIV (0.06 mg/ml; Sigma) at 37˚C. After enzymatic digestion, LA appendage was dissected into Kraftbrühe (KB) buffer containing KCl 25 mM, KH_2PO_4 10 mM, dextrose 20 mM, DL-aspartic acid potassium salt 10 mM, bovine albumin 0.1%, L-glutamic acid potassium salt 100 mM, $MgSO_4$ 2 mM, taurine 20 mM, EGTA 0.5 mM,

creatine 5 mM, HEPES 5 mM (pH 7.2). Single LA cardiomyocytes were dispersed by triturating the digested tissue and seeded on laminin-coated 8-mm coverslips. After 1 hour incubation at 37˚C in 5% CO_2 incubator, cardiomyocytes were treated with a gradually increased Ca^{2+} concentration from 0.06 mM to 1.2 mM in normal Tyrode's solution at RT.

Patch Clamping

Sodium currents (I_{Na}) were recorded by whole-cell patch-clamp techniques in isolated murine LA cardiomyocytes at RT using an established protocol.(84) Borosilicate-glass electrodes with tip-resistances 1.5-3 MΩ were filled with pipette solution. For I_{Na} recordings, pipette solution contained CsCl 135 mM, NaCl 10 mM, $CaCl_2$ 2 mM, EGTA 5 mM, HEPES 10 mM, MgATP 5 mM (pH 7.2 with CsOH); bath solution contained NaCl 50 mM, $CaCl_2$ 1.8 mM, MgCl2 1 mM, CsCl 110 mM, dextrose 10 mM, HEPES 10 mM, nifedipine 0.001 mM (pH 7.4 with CsOH). Currents were low pass filtered at 5 kHz with an Axopatch 200B amplifier and digitized at 10 kHz with a Digidata 1440A A/D converter. I_{Na} was obtained with 50-ms depolarizations (- 100 mV to + 40 mV) from a holding potential of - 120 mV at 0.1 Hz. Data were recorded with Clampex 10.3 and analyzed with Clampfit 10.3 (Molecular Devices Inc.). Cell-capacitance and series resistance were compensated by ~70%. Leakage compensation was not used. Currents were normalized to cell capacitance. (Obese SGK1 WT, 56±7 pF, N=7; obese SGK1 DN, 56±4 pF, N=8; p=NS). The I_{Na} reversal potential was derived by linear regression of the positive slop of the I-V relation: SGK1 WT, 37 ± 7 mV, SGK1 DN, 44 ± 7 mV; both were close to the Na^+ reversal potential by the Nernst equation (~40 mV).

Quantitative PCR of RNA

Tissue samples were snap frozen and then lysed using a Tissue Lyser (Qiagen) in TRIzol (Thermo Fisher) followed by RNA extraction. A total of 500ng of RNA was reverse transcribed using the High Capacity cDNA Reverse Transcription Kit (Thermo Fisher). Real-time PCR was conducted with SsoAdvance Universal SYBR Green (Bio-Rad) using a QuantStudio 6 Flex Real-Time PCR System (Thermo Fisher). Quantification of all target-gene expression was normalized to β-actin. Primers for genes of interest are presented in Supplemental Table 9.

RNA Sequencing

RNA isolation and reverse transcription were carried out as described above. Three samples each of lean and obese mouse atria were used to extract RNA, and quality was assessed with the RNA 6000 Pico assay kit using the Agilent Bioanalyzer. Sequencing-ready cDNA libraries were prepared using the NEBNext Ultra RNA Directional Library Prep kit for Illumina following the manufacturer's protocol. Bioanalyzer traces were used to confirm library size distribution. The libraries were quantified by qPCR using the KAPA Library Quantification kit and then sequenced as single-end 50 base reads on a Illimuna HiSeq 2000 in high-output mode.

The raw sequence image files from the sequencer were converted to the *fastq* format and checked for quality to ensure the sequencing quality scores did not deteriorate at the read ends. Useful metrics such as the per base sequence quality, the per base sequence content, per base N content, sequence length distribution, adapter and k-mer content and sequence duplication levels were collected for each sequencing run using *fastqc*.(85) At this stage, any samples that

did not pass QC were flagged and investigated later. The *fastqs* were then aligned to the mouse genome (GRCm38, ENSEMBL version 79) using *STAR*(86) aligner. The alignment files in the form of *bam* files were indexed for the ability to view them on Integrative Genome Viewer (IGV).(87) Alignment statistics such as average read length, percentage of uniquely mapped reads, percentage of multi-mapped reads and number of splice junctions were collated. Only reads that were uniquely mapped were considered for read annotation to gene features. Reads were annotated with the ENSEMBL 79 gene transfer format (gtf) file using *Salmon*.(88) *Salmon* provides both read counts and transcripts per million reads (TPMs) for each gene feature in the ENSEMBL gtf. The R package *DESeq2*(89) was used for differential gene expression analysis. Genes were considered differentially expressed if they were UP-regulated by log2FC > +1 or DOWN-regulated by log2FC < -1 with an FDR value < 0.05 (FC: fold change of average counts per million; FDR: false discovery rate).

Pathway analysis was performed using Gene Set Enrichment Analysis(90, 91) (GSEA preranked mode) using the KEGG pathway database. For all genes included in the differential expression analysis using DESeq2 (previously described) a metric was computed as the product of logFC and -log10(P-value). The genes were ranked by this metric resulting in the most significantly overexpressed genes at the top of the list and the most significantly under-expressed genes at the bottom. A "running sum" statistic was calculated for each gene set in the pathway database, based on the ranks of the members of the set, relative to those of the non-members. The enrichment score (ES) was defined as the maximum sum of the running sum and the genes that

made up this maximum ES contributed to the core enrichment in that pathway. All pathways with an FDR < 0.25 were considered significant.

Statistics

Data is reported as mean ± standard deviation, unless specifically noted otherwise. All statistical analyses were conducted with GraphPad Prism software. Animal group sizes were as low as possible. Categorical variables with binary outcomes were compared with the Fisher exact test. The Shapiro Wilks test of normality was utilized, and normality was rejected for $p<0.01$. For a comparison of two groups, a two-tailed Student's t-test (for normally distributed data) or a two-tailed Mann-Whitney test (where normality was rejected) were used to determine statistical significance. For comparisons of three normally distributed groups, a one-way ANOVA was performed, followed by post-hoc Dunnett's test. For comparisons of three groups where normal distribution could not be assumed, a Kruskal Wallis test was performed, and if significant, post-hoc Dunn testing was performed. A P-value <0.05 was used to denote statistical significance.

Study Approval

All studies were approved by the Institutional Animal Care and Use Committee (IACUC) and were in accordance with the NIH Guide for the Care and Use of Laboratory Animals.

AUTHOR CONTRIBUTIONS:

AB, SD, and DM conceived the studies; AB, MN, AR, PE, SD and DM designed the experiments; AB, GL, LX, AY, MH, JG, MY, MJS, YI, JT, and XY performed the experiments; AB, GL, LX, AY and MH analyzed the data; AB, SD, and DM wrote the manuscript.

ACKNOWLEDGEMENTS:

Dr. Aneesh Bapat was supported by the NIH grant T32HL007604. Dr. Ling Xiao was supported by AHA 20CDA35260081. Dr. Saumya Das was funded by AHA SFRN SFRN35120123 and AHA 18IPA34170109. Dr. Matthias Nahrendorf was supported by NIH grant R35 HL139598. Dr. Maximillian J. Schloss was supported by Deutsche Forschungsgemeinschaft (SCHL 2221/1-1). Dr. Ellinor is supported by grants from the National Institutes of Health (1RO1HL092577), by a grant from the American Heart Association Strategically Focused Research Networks (18SFRN34110082), and by a grant from the European Union (MAESTRIA 965286).

CONFLICTS OF INTEREST:

The authors declare that they have no relevant conflict of interest. SD, DM and AR are founding members of Long QT Therapeutics, which did not play any role in the funding or design of this study. M.N. has received funds or material research support from Alnylam, Biotronik, CSL Behring, GlycoMimetics, GSK, Medtronic, Novartis and Pfizer, as well as consulting fees from Biogen, Gimv, IFM Therapeutics, Molecular Imaging, Sigilon and Verseau Therapeutics. PTE has received sponsored research support from Bayer AG and IBM Research; he has also served on advisory boards or consulted for Bayer AG, MyoKardia and Novartis.

REFERENCES

1. Hales CM, Carroll MD, Fryar CD, Ogden CL. Prevalence of Obesity and Severe Obesity Among Adults: United States, 2017-2018. *NCHS Data Brief* 2020;(360):1–8.
2. Ogden CL et al. Trends in obesity prevalence by race and hispanic origin - 1999-2000 to 2017-2018. *JAMA - Journal of the American Medical Association* 2020;324(12):1208–1210.
3. Morin DP et al. The State of the Art: Atrial Fibrillation Epidemiology, Prevention, and Treatment. [Internet]. *Mayo Clin Proc* 2016;91(12):1778–1810.
4. Huxley RR et al. Absolute and Attributable Risks of Atrial Fibrillation in Relation to Optimal and Borderline Risk Factors: The Atherosclerosis Risk in Communities (ARIC) Study [Internet]. *Circulation* 2011;123(14):1501–1508.
5. Tedrow UB et al. The long- and short-term impact of elevated body mass index on the risk of new atrial fibrillation the WHS (women's health study).. *J Am Coll Cardiol* 2010;55(21):2319–27.
6. Lavie CJ, Pandey A, Lau DH, Alpert MA, Sanders P. Obesity and Atrial Fibrillation Prevalence, Pathogenesis, and Prognosis. *J Am Coll Cardiol* 2017;70(16):2022–2035.
7. Mahajan R et al. Electrophysiological, Electroanatomical, and Structural Remodeling of the Atria as Consequences of Sustained Obesity.. *J Am Coll Cardiol* 2015;66(1):1–11.
8. Abed HS et al. Obesity results in progressive atrial structural and electrical remodeling: implications for atrial fibrillation.. *Heart Rhythm* 2013;10(1):90–100.
9. Zhang F, Hartnett S, Sample A, Schnack S, Li Y. High fat diet induced alterations of atrial electrical activities in mice.. *Am J Cardiovasc Dis* 2016;6(1):1–9.
10. Fukui A et al. Hyperleptinemia Exacerbates High-Fat Diet-Mediated Atrial Fibrosis and Fibrillation.. *J Cardiovasc Electrophysiol* 2017;28(6):702–710.
11. Takahashi K et al. High-fat diet increases vulnerability to atrial arrhythmia by conduction disturbance via miR-27b.. *J Mol Cell Cardiol* 2016;90:38–46.
12. Meng T et al. Exposure to a chronic high-fat diet promotes atrial structure and gap junction remodeling in rats.. *Int J Mol Med* 2017;40(1):217–225.
13. Rheinheimer J, de Souza BM, Cardoso NS, Bauer AC, Crispim D. Current role of the NLRP3 inflammasome on obesity and insulin resistance: A systematic review.. *Metabolism* 2017;74:1–9.
14. Yao C et al. Enhanced Cardiomyocyte NLRP3 Inflammasome Signaling Promotes Atrial Fibrillation [Internet]. *Circulation* 2018;1.
15. Park J et al. Serum and glucocorticoid-inducible kinase (SGK) is a target of the PI 3-kinase-stimulated signaling pathway.. *EMBO J* 1999;18(11):3024–33.
16. Webster MK, Goya L, Ge Y, Maiyar AC, Firestone GL. Characterization of sgk, a novel member of the serine/threonine protein kinase gene family which is transcriptionally induced by glucocorticoids and serum.. *Mol Cell Biol* 1993;13(4):2031–40.
17. Neefs J, van den Berg NWE, Krul SPJ, Boekholdt SM, de Groot JR. Effect of Spironolactone on Atrial Fibrillation in Patients with Heart Failure with Preserved Ejection Fraction: Post-Hoc Analysis of the Randomized, Placebo-Controlled TOPCAT Trial. *American Journal of Cardiovascular Drugs* 2020;20(1):73–80.
18. Tsai CT et al. Increased Expression of Mineralocorticoid Receptor in Human Atrial Fibrillation and a Cellular Model of Atrial Fibrillation. *J Am Coll Cardiol* 2010;55(8):758–770.

19. Seccia TM et al. Arterial Hypertension, Atrial Fibrillation, and Hyperaldosteronism: The Triple Trouble. *Hypertension* 2017;69(4):545–550.
20. Swedberg K et al. Eplerenone and atrial fibrillation in mild systolic heart failure: Results from the EMPHASIS-HF (Eplerenone in Mild Patients Hospitalization and SurvIval Study in Heart Failure) study. *J Am Coll Cardiol* 2012;59(18):1598–1603.
21. Takemoto Y et al. Eplerenone Reduces Atrial Fibrillation Burden Without Preventing Atrial Electrical Remodeling. *J Am Coll Cardiol* 2017;70(23):2893–2905.
22. Reil JC et al. Aldosterone promotes atrial fibrillation. *European Heart Journal* 2012;33(16):2098–2108.
23. Liu T et al. Mineralocorticoid receptor antagonists and atrial fibrillation: A meta-analysis. *Europace* 2016;18(5):672–678.
24. Maria Z, Campolo AR, Scherlag BJ, Ritchey JW, Lacombe VA. Dysregulation of insulin-sensitive glucose transporters during insulin resistance-induced atrial fibrillation. *Biochimica et Biophysica Acta (BBA) - Molecular Basis of Disease* 2018;1864(4):987–996.
25. Scott TA, Babayeva O, Banerjee S, Zhong W, Francis SC. SGK1 is modulated by resistin in vascular smooth muscle cells and in the aorta following diet-induced obesity. *Obesity* 2016;24(3):678–686.
26. Schernthaner-Reiter MH et al. Strong association of serum- and glucocorticoid-regulated kinase 1 with peripheral and adipose tissue inflammation in obesity.. *Int J Obes (Lond)* 2015;39(7):1143–50.
27. Elahi M et al. High-fat diet-induced activation of SGK1 promotes Alzheimer's disease-associated tau pathology. *BioRxiv [preprint]* 2020;2507(1):1–9.
28. Wang C-Y, Liao JK. A mouse model of diet-induced obesity and insulin resistance.. *Methods Mol Biol* 2012;821:421–33.
29. Aoyama T et al. Serum and glucocorticoid-responsive kinase-1 regulates cardiomyocyte survival and hypertrophic response. *Circulation* 2005;111(13):1652–1659.
30. Das S et al. Pathological role of serum- and glucocorticoid-regulated kinase 1 in adverse ventricular remodeling.. *Circulation* 2012;126(18):2208–19.
31. Yang M et al. Serum-glucocorticoid regulated kinase 1 regulates alternatively activated macrophage polarization contributing to angiotensin II-induced inflammation and cardiac fibrosis.. *Arterioscler Thromb Vasc Biol* 2012;32(7):1675–86.
32. Gan W et al. The SGK1 inhibitor EMD638683, prevents Angiotensin II–induced cardiac inflammation and fibrosis by blocking NLRP3 inflammasome activation. *Biochimica et Biophysica Acta - Molecular Basis of Disease* 2018;1864(1):1–10.
33. Lin YKYJ et al. Leptin modulates electrophysiological characteristics and isoproterenol-induced arrhythmogenesis in atrial myocytes. *Journal of Biomedical Science* 2013;20(1):1–9.
34. Chadda KR, Jeevaratnam K, Lei M, Huang CLH. Sodium channel biophysics, late sodium current and genetic arrhythmic syndromes. *Pflugers Archiv European Journal of Physiology* 2017;469(5–6):629–641.
35. McCauley MD et al. *Ion Channel and Structural Remodeling in Obesity-Mediated Atrial Fibrillation*. 2020:
36. Scott L et al. NLRP3 inflammasome is a key driver of obesity-induced atrial arrhythmias. *Cardiovascular Research* 2021;117(7):1746–1759.

37. Spinale FG. Myocardial Matrix Remodeling and the Matrix Metalloproteinases: Influence on Cardiac Form and Function. *Physiological Reviews* 2007;87(4):1285–1342.
38. Kassiri Z, Khokha R. Myocardial extra-cellular matrix and its regulation by metalloproteinases and their inhibitors.. *Thromb Haemost* 2005;93(2):212–9.
39. Jansen HJ et al. Atrial structure, function and arrhythmogenesis in aged and frail mice.. *Sci Rep* 2017;7(March):44336.
40. Harada M, Nattel S. Implications of Inflammation and Fibrosis in Atrial Fibrillation Pathophysiology. *Cardiac Electrophysiology Clinics* 2021;13(1):25–35.
41. Brem AS, Morris DJ, Gong R. Aldosterone-induced fibrosis in the kidney: questions and controversies.. *Am J Kidney Dis* 2011;58(3):471–9.
42. Chen B et al. Mineralocorticoid receptor: A hidden culprit for hemodialysis vascular access dysfunction.. *EBioMedicine* 2019;39:621–627.
43. Mouton AJ, Li X, Hall ME, Hall JE. Obesity, hypertension, and cardiac dysfunction novel roles of immunometabolism in macrophage activation and inflammation. *Circulation Research* 2020;789–806.
44. Yao L, Herlea-Pana O, Heuser-Baker J, Chen Y, Barlic-Dicen J. Roles of the chemokine system in development of obesity, insulin resistance, and cardiovascular disease. *Journal of Immunology Research* 2014;2014. doi:10.1155/2014/181450
45. Vallon V et al. SGK1-dependent cardiac CTGF formation and fibrosis following DOCA treatment. *Journal of Molecular Medicine* 2006;84(5):396–404.
46. Belaiba RS et al. The serum- and glucocorticoid-inducible kinase Sgk-1 is involved in pulmonary vascular remodeling: Role in redox-sensitive regulation of tissue factor by thrombin. *Circulation Research* 2006;98(6):828–836.
47. Zhang L, Cui R, Cheng X, Du J. Antiapoptotic effect of serum and glucocorticoid-inducible protein kinase is mediated by novel mechanism activating IκB kinase. *Cancer Research* 2005;65(2):457–464.
48. Bauernfeind FG et al. Cutting Edge: NF-κB Activating Pattern Recognition and Cytokine Receptors License NLRP3 Inflammasome Activation by Regulating NLRP3 Expression. *The Journal of Immunology* 2009;183(2):787–791.
49. Tai DJC, Su CC, Ma YL, Lee EHY. SGK1 phosphorylation of IκB kinase α and p300 up-regulates NF-κB activity and increases N-methyl-D-aspartate receptorNR2A and NR2B expression. *Journal of Biological Chemistry* 2009;284(7):4073–4089.
50. Chen LF, Greene WC. Shaping the nuclear action of NF-κB. *Nature Reviews Molecular Cell Biology* 2004;5(5):392–401.
51. Viatour P, Merville MP, Bours V, Chariot A. Phosphorylation of NF-κB and IκB proteins: Implications in cancer and inflammation. *Trends in Biochemical Sciences* 2005;30(1):43–52.
52. Men L et al. Cardiac transcriptome analysis reveals nr4a1 mediated glucose metabolism dysregulation in response to high-fat diet. *Genes (Basel)* 2020;11(7):1–15.
53. Zhou B et al. Serum- and glucocorticoid-induced kinase drives hepatic insulin resistance by directly inhibiting AMP-activated protein kinase. [Internet]. *Cell Rep* 2021;37(1):109785.
54. Zhang M et al. Serum- and glucocorticoid-inducible kinase 1 promotes insulin resistance in adipocytes via degradation of insulin receptor substrate 1. [Internet]. *Diabetes Metab Res Rev* 2021;37(4):e3451.

55. Lang F, Shumilina E. Regulation of ion channels by the serum- and glucocorticoid-inducible kinase SGK1. *FASEB Journal* 2013;27(1):3–12.
56. Schile AJ. Jaxpheno11: Early stages of type 2 diabetes in C57BL/6J male mice on a high-fat diet [Internet]. *Mouse Phenome Database at The Jackson Laboratory* 2017;https://phenome.jax.org/projects/Jaxpheno11. cited
57. Lin YK et al. A monounsaturated fatty acid (oleic acid) modulates electrical activity in atrial myocytes with calcium and sodium dysregulation. *International Journal of Cardiology* 2014;176(1):191–198.
58. Biet M et al. Lasting alterations of the sodium current by short-term hyperlipidemia as a mechanism for initiation of cardiac remodeling. *American Journal of Physiology - Heart and Circulatory Physiology* 2014;306(2):291–297.
59. O'Connell RP et al. Free fatty acid effects on the atrial myocardium: Membrane ionic currents are remodeled by the disruption of T-tubular architecture. *PLoS ONE* 2015;10(8):1–18.
60. Wu CC, Su MJ, Chi JF, Wu MH, Lee YT. Comparison of aging and hypercholesterolemic effects on the sodium inward currents in cardiac myocytes. *Life Sciences* 1997;61(16):1539–1551.
61. Makiyama T et al. A Novel SCN5A Gain-of-Function Mutation M1875T Associated With Familial Atrial Fibrillation. *J Am Coll Cardiol* 2008;52(16):1326–1334.
62. Ziyadeh-Isleem A et al. A truncating SCN5A mutation combined with genetic variability causes sick sinus syndrome and early atrial fibrillation [Internet]. *Heart Rhythm* 2014;11(6):1015–1023.
63. Ornelas-Loredo A et al. Association between Obesity-Mediated Atrial Fibrillation and Therapy with Sodium Channel Blocker Antiarrhythmic Drugs. *JAMA Cardiology* 2020;5(1):57–64.
64. Avula UMR et al. Attenuating persistent sodium current induced atrial myopathy and fibrillation by preventing mitochondrial oxidative stress. [Internet]. *JCI Insight* [published online ahead of print: 2021]; doi:10.1172/jci.insight.147371
65. Lang F et al. (Patho)physiological significance of the serum- and glucocorticoid- inducible kinase isoforms. *Physiological Reviews* 2006;86(4):1151–1178.
66. Kim JB et al. Polony multiplex analysis of gene expression (PMAGE) in mouse hypertrophic cardiomyopathy. [Internet]. *Science* 2007;316(5830):1481–4.
67. Rickard AJ et al. Cardiomyocyte mineralocorticoid receptors are essential for deoxycorticosterone/salt-mediated inflammation and cardiac fibrosis. *Hypertension* 2012;60(6):1443–1450.
68. Leroy V et al. Aldosterone activates NF-κB in the collecting duct. *Journal of the American Society of Nephrology* 2009;20(1):131–144.
69. Voelkl J et al. SGK1 induces vascular smooth muscle cell calcification through NF-?B signaling. *Journal of Clinical Investigation* 2018;128(7):3024–3040.
70. Xi X et al. SGK1 Mediates Hypoxic Pulmonary Hypertension through Promoting Macrophage Infiltration and Activation2019;2019.
71. Heras-Bautista CO et al. Cardiomyocytes facing fibrotic conditions re-express extracellular matrix transcripts. *Acta Biomaterialia* 2019;89:180–192.
72. Schram K et al. Leptin regulates MMP-2, TIMP-1 and collagen synthesis via p38 MAPK in HL-1 murine cardiomyocytes. *Cellular and Molecular Biology Letters* 2010;15(4):551–563.

73. Koitabashi N et al. Pivotal role of cardiomyocyte TGF-β signaling in the murine pathological response to sustained pressure overload. *Journal of Clinical Investigation* 2011;121(6):2301–2312.
74. Suetomi T et al. Inflammation and NLRP3 Inflammasome Activation Initiated in Response to Pressure Overload by CaMKII δ Signaling in Cardiomyocytes are Essential for Adverse Cardiac Remodeling2018;(858):2530–2544.
75. Willeford A et al. CaMKIIδ-mediated inflammatory gene expression and inflammasome activation in cardiomyocytes initiate inflammation and induce fibrosis. *JCI Insight* 2018;3(12). doi:10.1172/jci.insight.97054
76. Lindsey ML, Kassiri Z, Virag JAI, de Castro Brás LE, Scherrer-Crosbie M. Guidelines for measuring cardiac physiology in mice. [Internet]. *Am J Physiol Heart Circ Physiol* 2018;314(4):H733–H752.
77. Wilde E et al. Tail-Cuff Technique and Its Influence on Central Blood Pressure in the Mouse. [Internet]. *J Am Heart Assoc* 2017;6(6). doi:10.1161/JAHA.116.005204
78. Enriori PJ et al. Diet-Induced Obesity Causes Severe but Reversible Leptin Resistance in Arcuate Melanocortin Neurons. *Cell Metabolism* 2007;5(3):181–194.
79. Grune J et al. Evaluation of a commercial multi-dimensional echocardiography technique for ventricular volumetry in small animals.. *Cardiovasc Ultrasound* 2018;16(1):10.
80. Grune J et al. Selective Mineralocorticoid Receptor Cofactor Modulation as Molecular Basis for Finerenone's Antifibrotic Activity.. *Hypertension* 2018;71(4):599–608.
81. Mahida S et al. Overexpression of KCNN3 results in sudden cardiac death.. *Cardiovasc Res* 2014;101(2):326–34.
82. Glukhov A V, Flagg TP, Fedorov V, Efimov IR, Nichols CG. Differential K(ATP) channel pharmacology in intact mouse heart.. *J Mol Cell Cardiol* 2010;48(1):152–60.
83. Glukhov A V, Fedorov V, Anderson ME, Mohler PJ, Efimov IR. Functional anatomy of the murine sinus node: high-resolution optical mapping of ankyrin-B heterozygous mice.. *Am J Physiol Heart Circ Physiol* 2010;299(2):H482-91.
84. Ma J et al. High purity human-induced pluripotent stem cell-derived cardiomyocytes: electrophysiological properties of action potentials and ionic currents. [Internet]. *Am J Physiol Heart Circ Physiol* 2011;301(5):H2006-17.
85. Andrews S. FastQC: A quality control tool for high throughput sequence data. [Internet]https://www.bioinformatics.babraham.ac.uk/projects/fastqc/. cited
86. Dobin A et al. STAR: ultrafast universal RNA-seq aligner. [Internet]. *Bioinformatics* 2013;29(1):15–21.
87. Robinson JT et al. Integrative genomics viewer. [Internet]. *Nat Biotechnol* 2011;29(1):24–6.
88. Patro R, Duggal G, Love MI, Irizarry RA, Kingsford C. Salmon provides fast and bias-aware quantification of transcript expression. [Internet]. *Nat Methods* 2017;14(4):417–419.
89. Love MI, Huber W, Anders S. Moderated estimation of fold change and dispersion for RNA-seq data with DESeq2. [Internet]. *Genome Biol* 2014;15(12):550.
90. Subramanian A et al. Gene set enrichment analysis: a knowledge-based approach for interpreting genome-wide expression profiles. [Internet]. *Proc Natl Acad Sci U S A* 2005;102(43):15545–50.
91. Mootha VK et al. PGC-1alpha-responsive genes involved in oxidative phosphorylation are coordinately downregulated in human diabetes. [Internet]. *Nat Genet* 2003;34(3):267–73.

Figures and Figure Legends:

Figure 1: Diet induced obesity results in increased AF inducibility and is associated with upregulation of SGK1 signaling. ***A*** Schematic of HFD feeding in wild type mice to generate obese wild type mice. ***B*** Glucose levels after glucose tolerance test in lean and obese mice. ***C*** AF inducibility in lean and obese mice after specified period of feeding control or HFD chow. ***D*** Heatmap derived from RNA sequencing data demonstrating GSEA core-enriched genes in SGK1-related pathways (Family-wise error rate P<0.05) that are differentially expressed (Nominal P<0.05). ***E*** Atrial SGK1 mRNA expression in obese versus lean mice (left) and expression of phosphorylated (pSGK1), total SGK1 protein, and ratio as quantified by Western blotting (right). ***F*** Ventricular SGK1 mRNA expression in obese versus lean mice (left) and expression of phosphorylated (pSGK1), total SGK1 protein, and ratio as quantified by Western blotting (right). **G** Atrial expression of SGK1 phosphorylation targets NDRG1 and GSK3β in obese versus lean mice. The NDRG1 and GSK3β blots were from the same gel, so share a vinculin loading control. ***H*** Ventricular expression of SGK1 phosphorylation targets NDRG1 and GSK3β in obese versus lean mice. The NDRG1 and GSK3β blots were from the same gel, so share a vinculin loading control. For all parts of Figure 1, unpaired Student's t-test. *P<0.05, **P<0.01, and ***P<0.001. Number of mice in each group provided in legend, bar graph, or represented by the number of dots in individual figure.

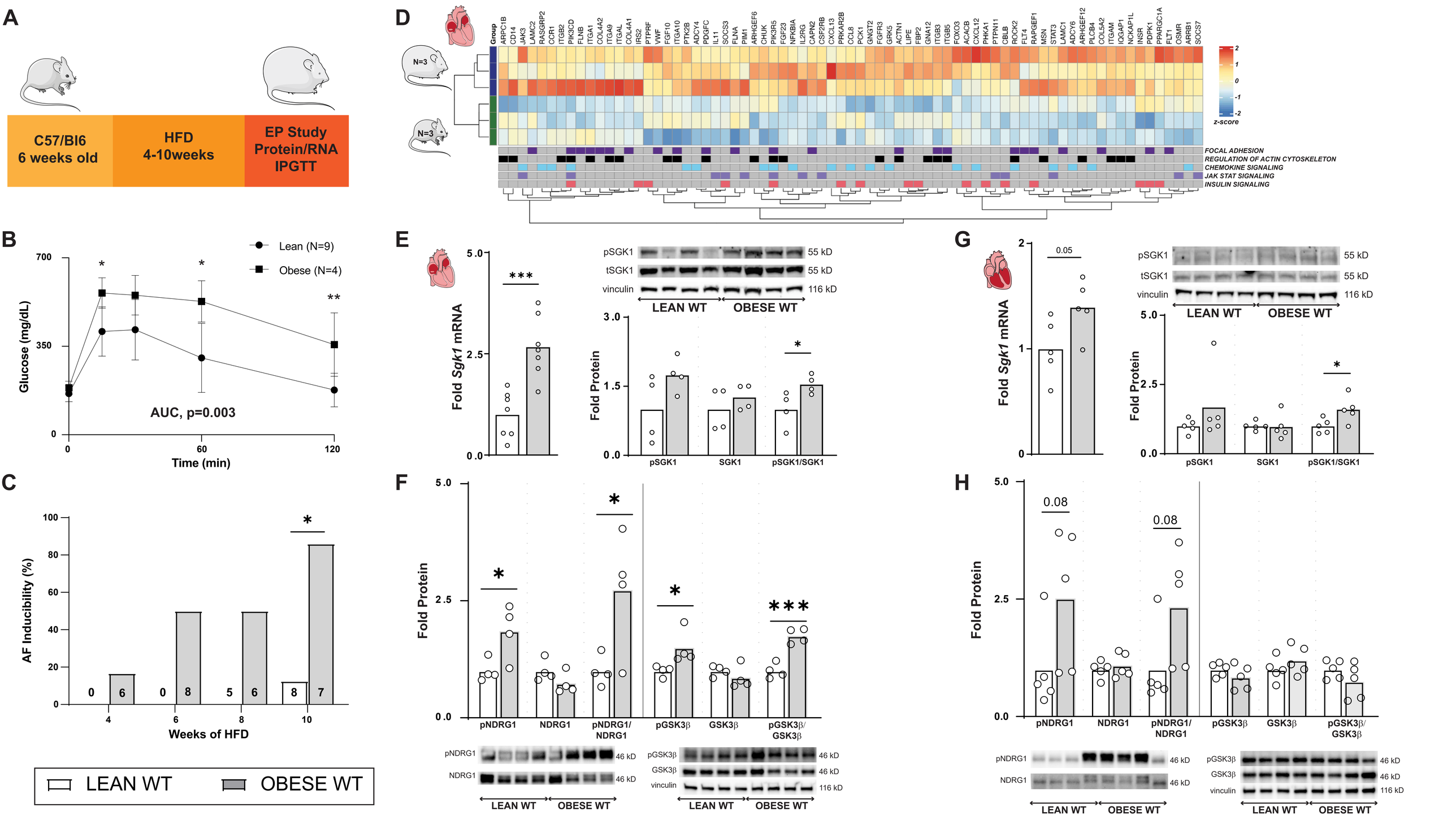
A
C57/Bl6
6 weeks old
HFD
4-10weeks
EP Study
Protein/RNA
IPGTT
B
Lean (N=9)
Obese (N=4)
Glucose (mg/dL)
700
350
0
0
60
120
Time (min)
AUC, p=0.003
C
AF Inducibility (%)
100
80
60
40
20
0
0 6 0 8 5 6 8 7
4
6
8
10
Weeks of HFD
LEAN WT
OBESE WT
D
Group
N=3
N=3
ARPC1B CD14 JAK3 LAMC2 RASGRP2 CCR1 ITGB2 PIK3CD FLNB ITGA1 COL4A2 ITGA9 ITGAL COL4A1 IRS2 PTPRF VWF FGF10 ITGA10 PTK2B ADCY4 PDGFC IL11 SOCS3 FLNA PIM1 ARHGEF6 CHUK PIK3R5 FGF23 NFKBIA IL2RG CAPN2 CSF2RB CXCL13 PRKAR2B CCL8 PCK1 GNGT2 FGFR3 GRK5 ACTN1 LIPE FBP2 GNA12 ITGB3 ITGB5 FOXO3 ACACB CXCL12 PHKA1 PTPN11 CBLB ROCK2 FLT4 RAPGEF1 MSN STAT3 LAMC1 ADCY6 ARHGEF12 PLCB4 COL5A2 ITGAM IQGAP1 NCKAP1L INSR PDPK1 PPARGC1A FLT1 OSMR ARRB1 SOCS7
2
1
0
-1
-2
z-score
FOCAL ADHESION
REGULATION OF ACTIN CYTOSKELETON
CHEMOKINE SIGNALING
JAK STAT SIGNALING
INSULIN SIGNALING
E
Fold Sgk1 mRNA
5.0
2.5
0.0
***
pSGK1
tSGK1
vinculin
55 kD
55 kD
116 kD
LEAN WT
OBESE WT
Fold Protein
3.0
1.5
0.0
*
pSGK1
SGK1
pSGK1/SGK1
F
Fold Protein
5.0
2.5
0.0
* * * ***
pNDRG1
NDRG1
pNDRG1/ NDRG1
pGSK3β
GSK3β
pGSK3β/ GSK3β
pNDRG1
NDRG1
46 kD
46 kD
pGSK3β
GSK3β
vinculin
46 kD
46 kD
116 kD
LEAN WT
OBESE WT
LEAN WT
OBESE WT
G
Fold Sgk1 mRNA
2
1
0
0.05
pSGK1
tSGK1
vinculin
55 kD
55 kD
116 kD
LEAN WT
OBESE WT
Fold Protein
5.0
2.5
0.0
*
pSGK1
SGK1
pSGK1/SGK1
H
Fold Protein
5.0
2.5
0.0
0.08
0.08
pNDRG1
NDRG1
pNDRG1/ NDRG1
pGSK3β
GSK3β
pGSK3β/ GSK3β
pNDRG1
NDRG1
46 kD
46 kD
pGSK3β
GSK3β
vinculin
46 kD
46 kD
116 kD
LEAN WT
OBESE WT
LEAN WT
OBESE WT

Figure 2: SGK1 DN mice are protected from obesity-induced AF. ***A*** Schematic of mouse model used in these studies. ***B*** Frequency of premature atrial complexes (PACs) recorded during continuous telemetry recordings over an 8-hour period. Below the quantified plot is a representative telemetry tracing; the red star identifies an ectopic atrial P wave and the dark blue scale bar is 100ms. The green plot graphs heart rate (bpm) during the tracing of interest. Unpaired Student's t-test. *P<0.05. ***C*** Example surface EKG and intracardiac tracing showing pacing-induced AF. ***D*** AF inducibility, by percent inducible, of lean and obese mice (left), total summed duration of all AF episodes during each EP study (middle) and number of episodes of induced AF > 250ms in duration by mouse (right). Fisher exact test for AF inducibility and Kruskal Wallis test with post-hoc Dunn's Test for duration/burden. *P<0.05, **P<0.01. Number of mice in each group is provided in bar graph or represented by the number of dots in individual figure.

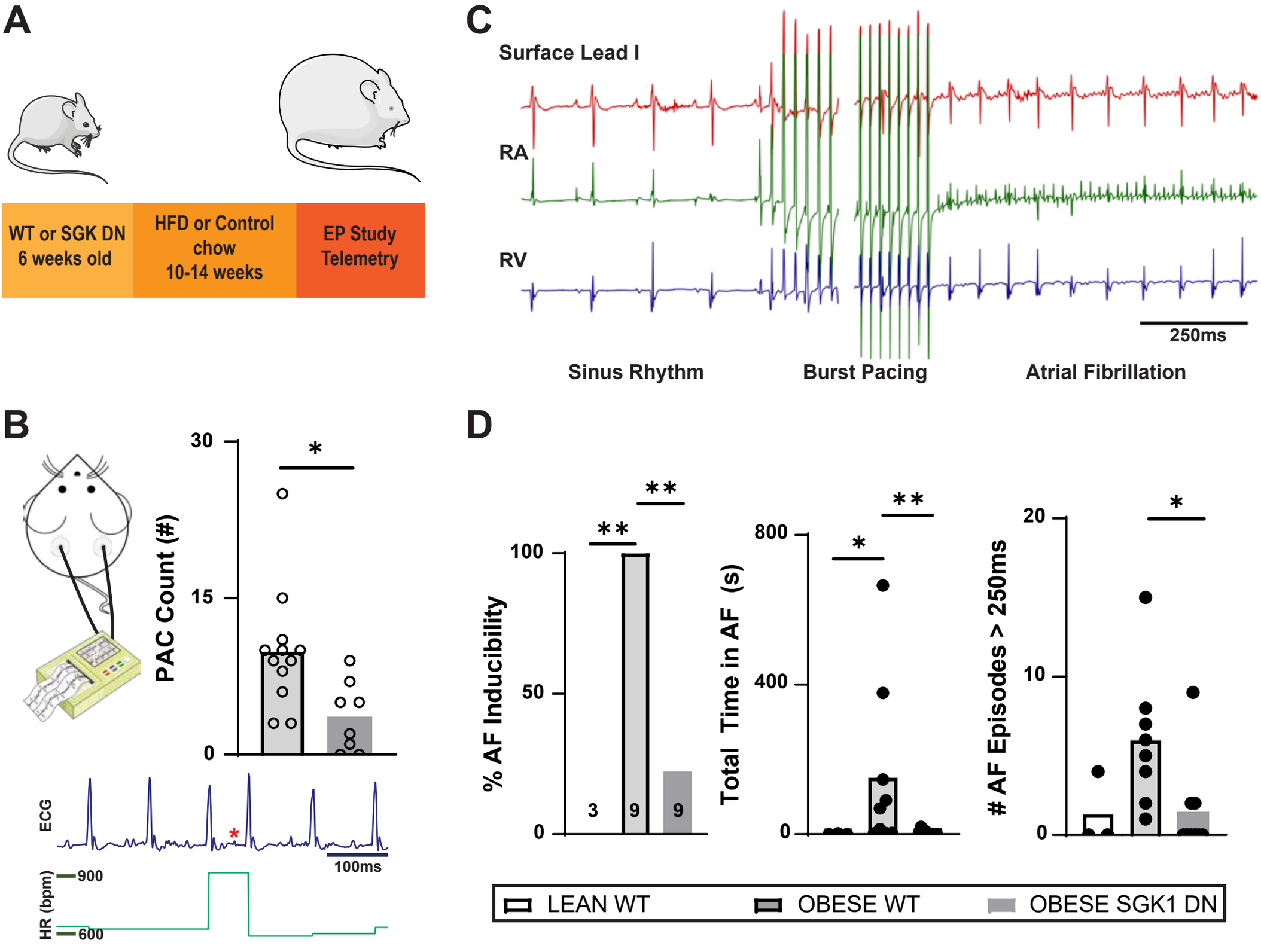
A
WT or SGK DN
6 weeks old
HFD or Control
chow
10-14 weeks
EP Study
Telemetry
C
Surface Lead I
RA
RV
250ms
Sinus Rhythm
Burst Pacing
Atrial Fibrillation
B
PAC Count (#)
30
15
0
*
ECG
100ms
HR (bpm)
900
600
D
% AF Inducibility
100
50
0
**
**
3
9
9
Total Time in AF (s)
800
400
0
*
**
AF Episodes > 250ms
20
10
0
*
LEAN WT
OBESE WT
OBESE SGK1 DN

Figure 3: Atrial electrophysiologic effects of SGK1 genetic inhibition on obese mice. ***A*** Right (upper) and left (lower) atrial action potential durations at 90% repolarization in lean and obese wild type and obese SGK1 DN mice. Tracings show representative optical action potential tracings. One-way ANOVA, Dunnett's test. *P<0.05. ***B*** Interatrial differences in APD at 50% repolarization (top), conduction velocity (middle), and upstroke velocity (dV/dt, bottom) in lean WT (left), obese WT (middle) and SGK1 DN (right) mouse atrial chambers. Paired student's t-test. *P<0.05, **P<0.01. ***C*** Representative blots and quantification of right (RA) and left (LA) atrial expression of phosphorylated SGK1 (pSGK1), total SGK1 (tSGK1) and the ratio of phosphorylated to total SGK1 (pSGK1/tSGK1) in lean (left) and obese (right) atria. Paired Student's t-test. *P<0.05, **P<0.05. Number of mice in each group is represented by the number of dots in individual figure.

A

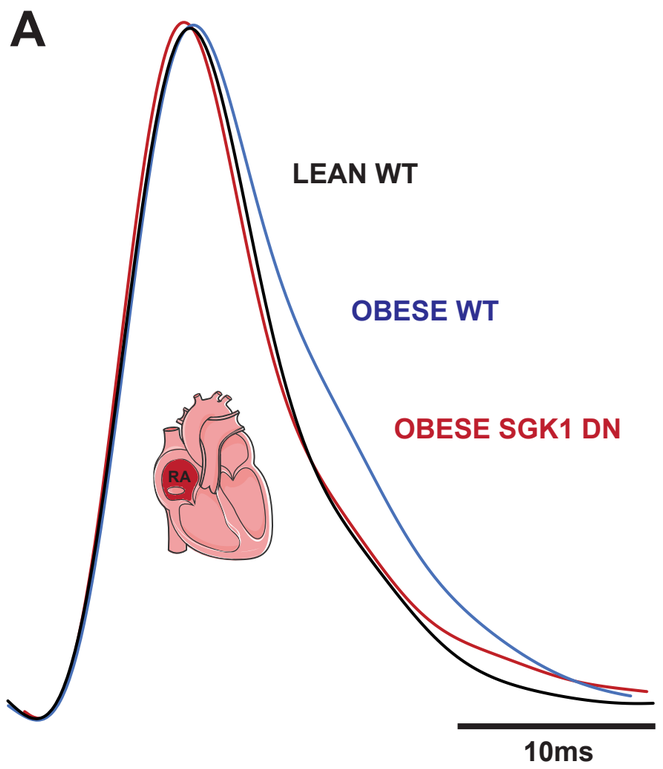
LEAN WT
OBESE WT
OBESE SGK1 DN
RA
10ms

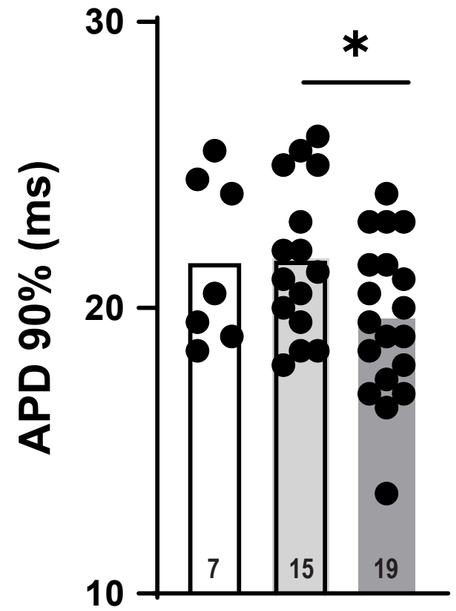
APD 90% (ms)
30
20
10
*
7
15
19

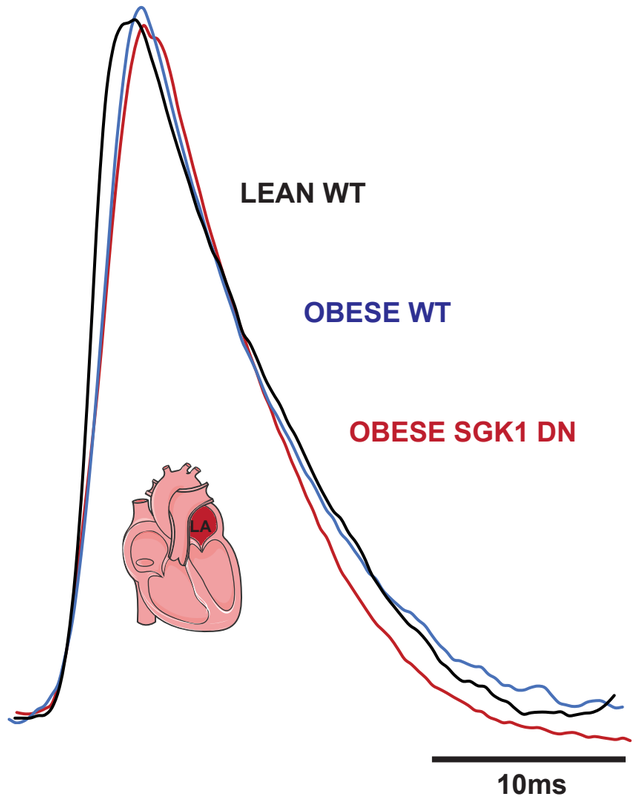
LEAN WT
OBESE WT
OBESE SGK1 DN
LA
10ms

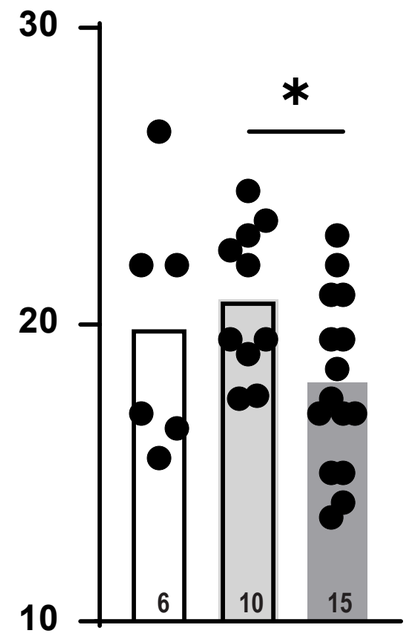
APD 90% (ms)
30
20
10
*
6
10
15


LEAN WT
OBESE WT
OBESE SGK1 DN

B

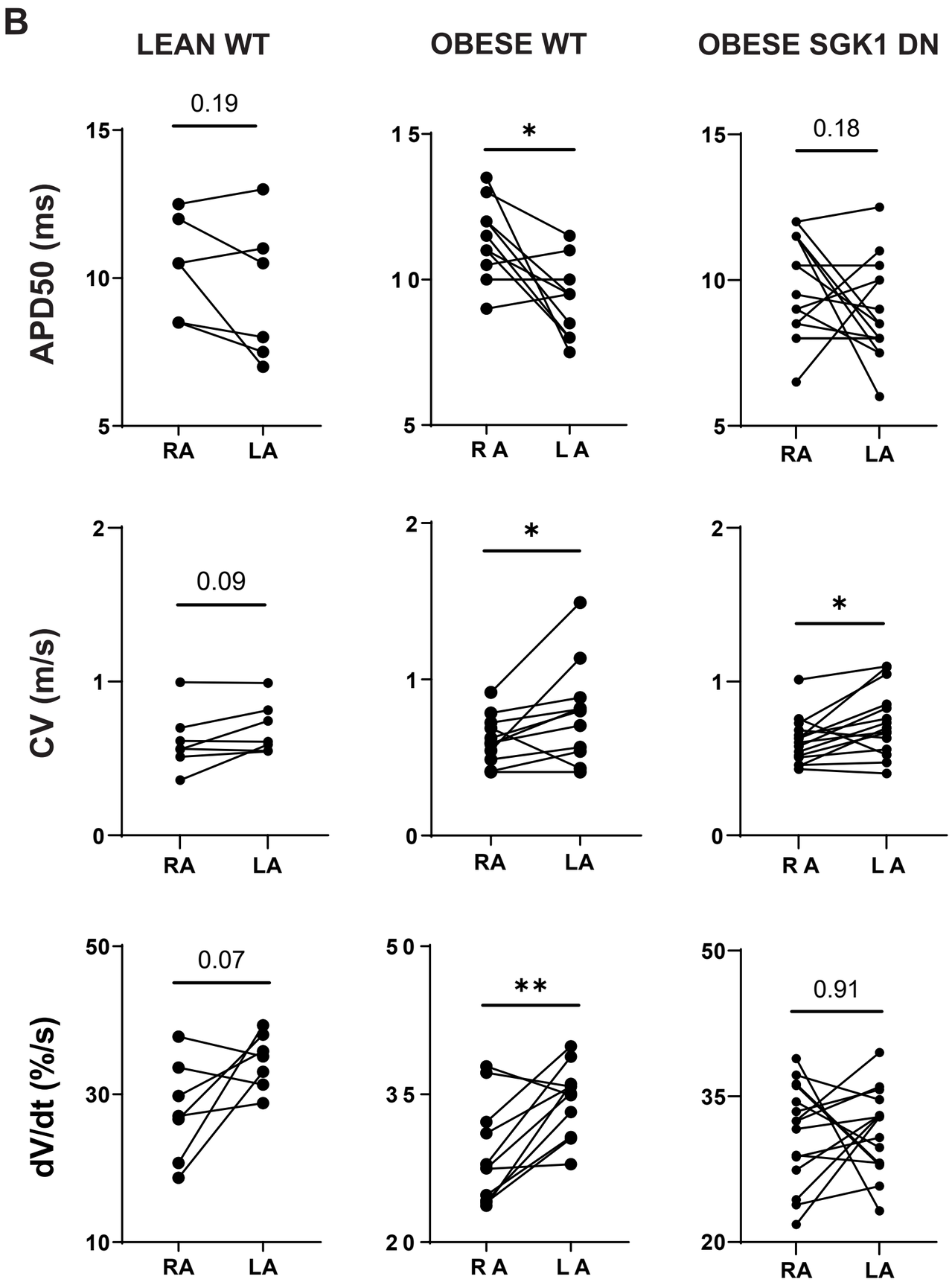
LEAN WT
OBESE WT
OBESE SGK1 DN
APD50 (ms)
0.19
*
0.18
CV (m/s)
0.09
*
*
dV/dt (%/s)
0.07
**
0.91
RA
LA

C

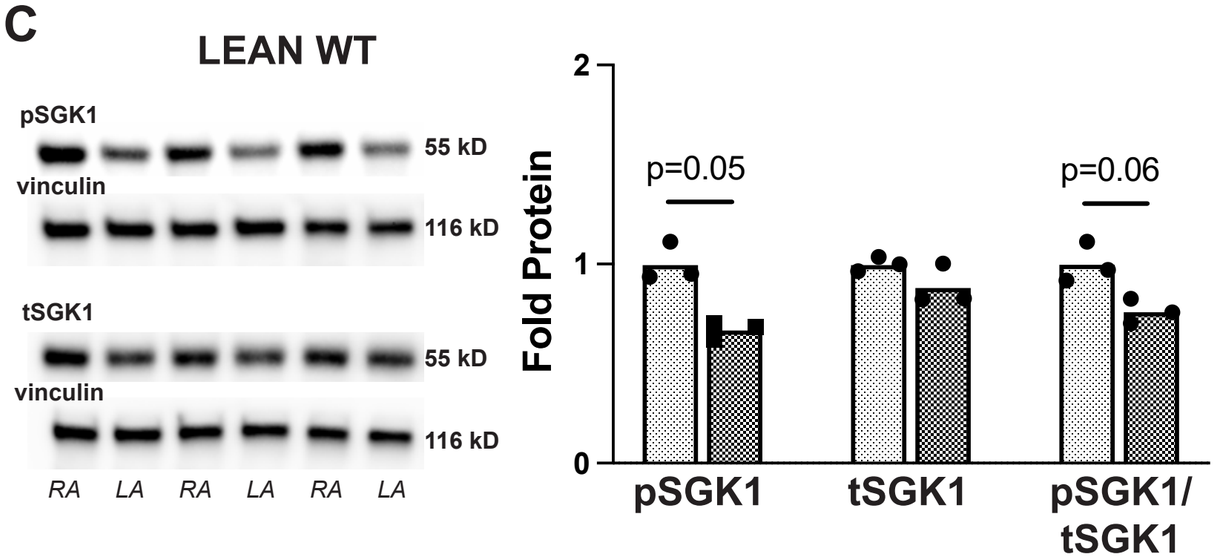
LEAN WT
pSGK1
55 kD
vinculin
116 kD
tSGK1
55 kD
vinculin
116 kD
RA LA RA LA RA LA
Fold Protein
p=0.05
p=0.06
pSGK1
tSGK1
pSGK1/
tSGK1

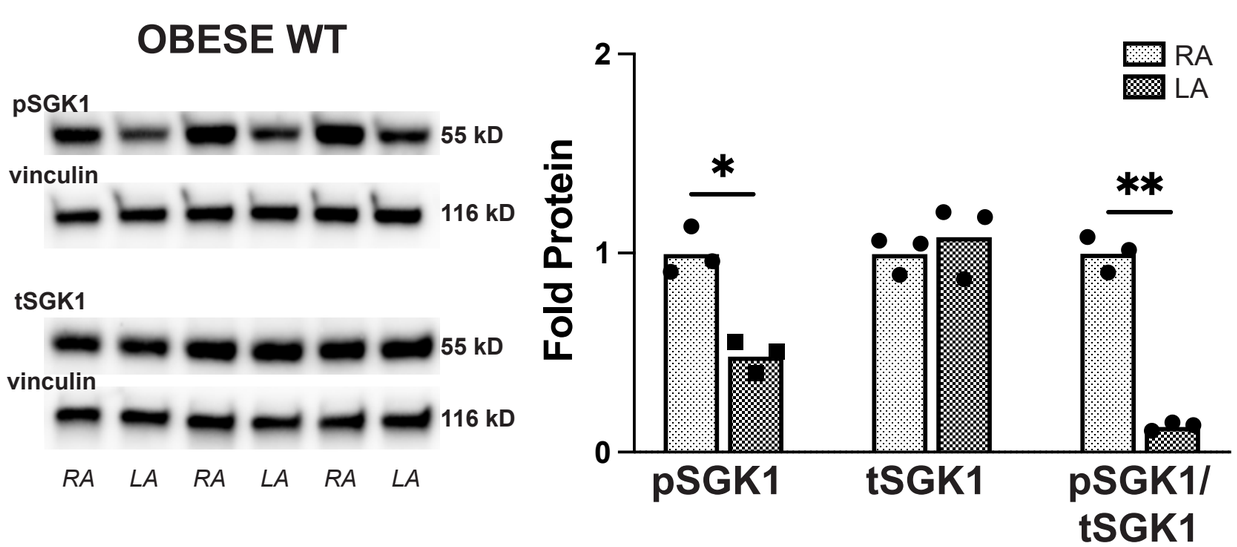
OBESE WT
pSGK1
55 kD
vinculin
116 kD
tSGK1
55 kD
vinculin
116 kD
RA LA RA LA RA LA
Fold Protein
RA
LA
*
**
pSGK1
tSGK1
pSGK1/
tSGK1

Figure 4: Effect of SGK1 genetic inhibition on I_{Na} in obese left atrial cardiomyocytes. *A* Example sodium current recordings from isolated left atrial (LA) cardiomyocytes of obese WT and SGK1 DN mice. ***B*** Current-voltage relations in wild type (black) and SGK1 DN (red) isolated LA. ***C*** I_{Na} activation-inactivation voltage dependences for WT (black) and SGK1 DN (red) left atrial cardiomyocytes, demonstrating a rightward depolarizing shift in the SGK1 DN myocytes. ***D*** Atrial expression of NaV1.5 subunit with representative blots below. In *B* and *C,* data depicted as mean $\pm$ SEM. Number of mice in each group provided in legend or represented by the number of dots in individual figure.

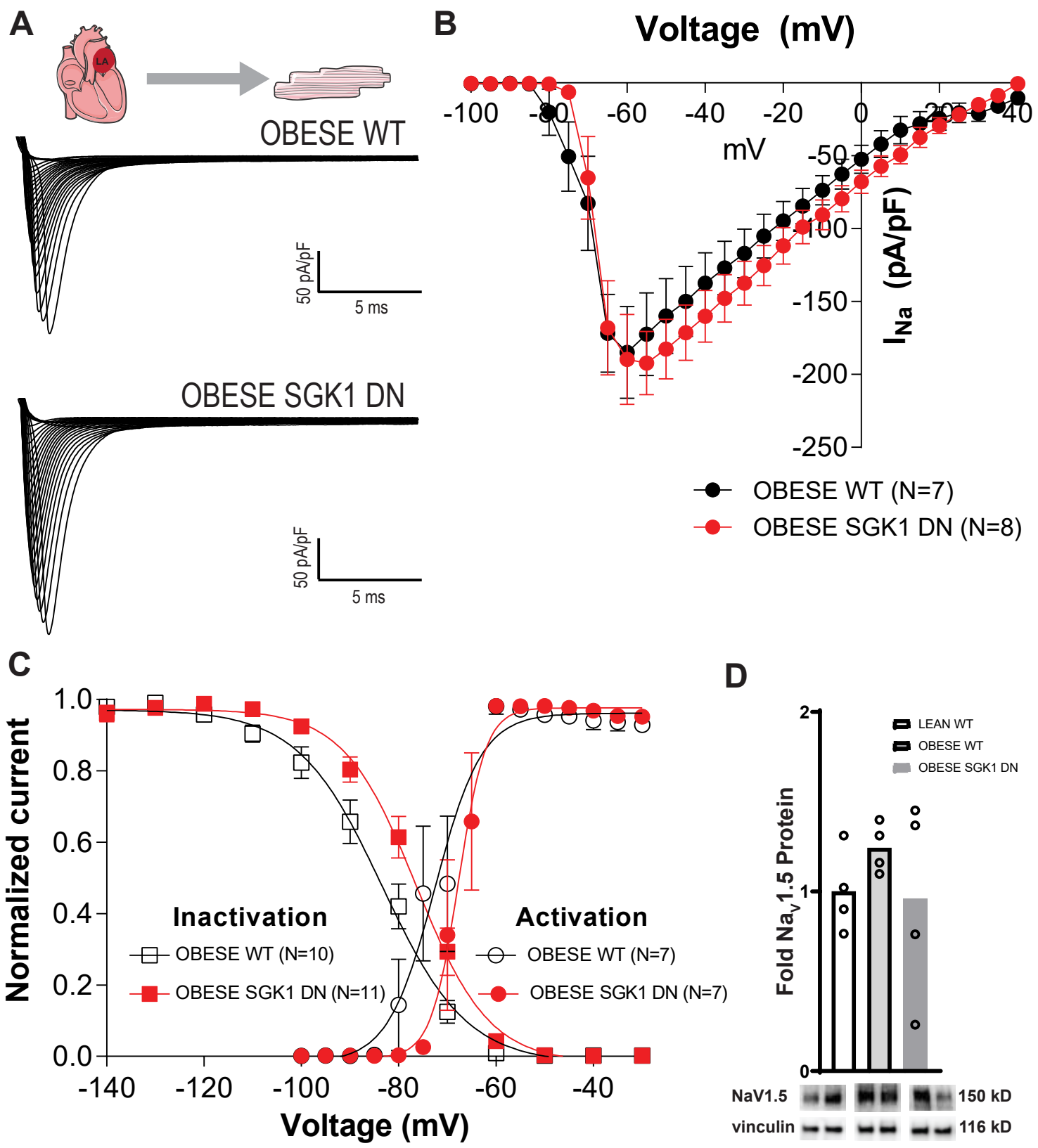
A
LA
OBESE WT
50 pA/pF
5 ms
OBESE SGK1 DN
50 pA/pF
5 ms
B
Voltage (mV)
-100
-80
-60
-40
-20
0
20
40
mV
-50
-100
-150
-200
-250
I_{Na} (pA/pF)
OBESE WT (N=7)
OBESE SGK1 DN (N=8)
C
Normalized current
1.0
0.8
0.6
0.4
0.2
0.0
Inactivation
OBESE WT (N=10)
OBESE SGK1 DN (N=11)
Activation
OBESE WT (N=7)
OBESE SGK1 DN (N=7)
-140
-120
-100
-80
-60
-40
Voltage (mV)
D
Fold $Na_V1.5$ Protein
2
1
0
LEAN WT
OBESE WT
OBESE SGK1 DN
NaV1.5
150 kD
vinculin
116 kD

Figure 5: SGK1 genetic inhibition prevents obesity-induced atrial fibrotic signaling. *A* Expression of fibrosis-related genes in lean and obese atria and ventricles. One-way ANOVA, Dunnett's test or Kruskal-Wallis, Dunn's test (only LV TIMP1/MMP2, LV TIMP1/MMP9). *P<0.05, **P<0.01, ***P<0.001, ****P<0.0001. ***B*** Atrial CTGF protein expression with representative blots. One-way ANOVA, Dunnett's test. *P<0.05. ***C*** Connexin protein expression measured by Western Blot, with representative blots. One-way ANOVA, Dunnett's test. *P<0.05, **P<0.01. ***D*** Expression of connexin 40 (above) and 43(below) mRNA transcripts. One-way ANOVA, Dunnett's test. *P<0.05, **P<0.01. Number of mice in each group is represented by the number of dots in individual figure.

A

Fold mRNA

Ctgf | αsma | Col1A1 | Tgf-β | Timp1/Mmp2 | Timp1/Mmp9

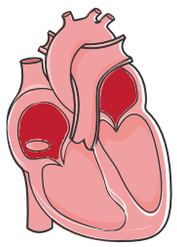

ANOVA p 0.06 | 0.05 | * | * | * | * | *

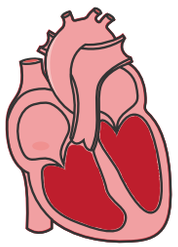

*** | **** | **** | *** | ** | **

B

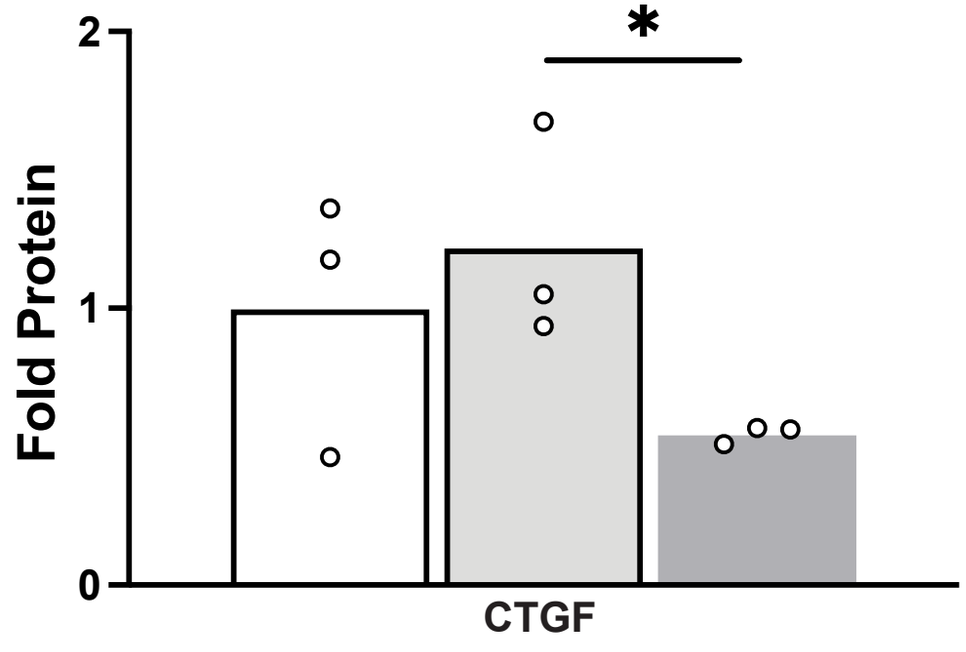

C

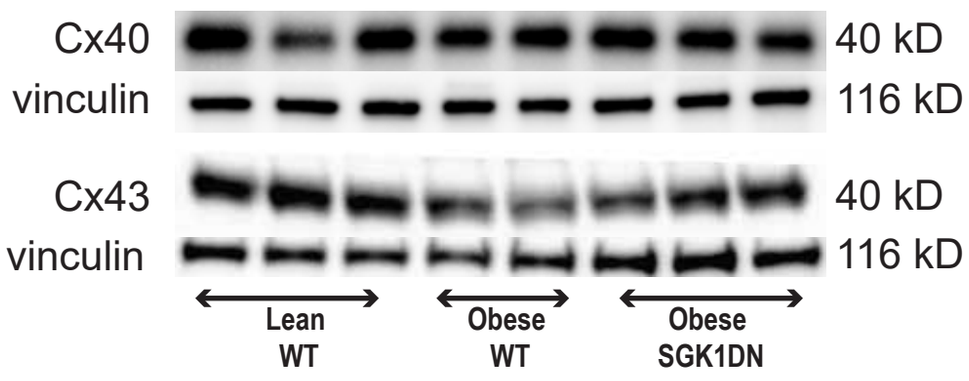

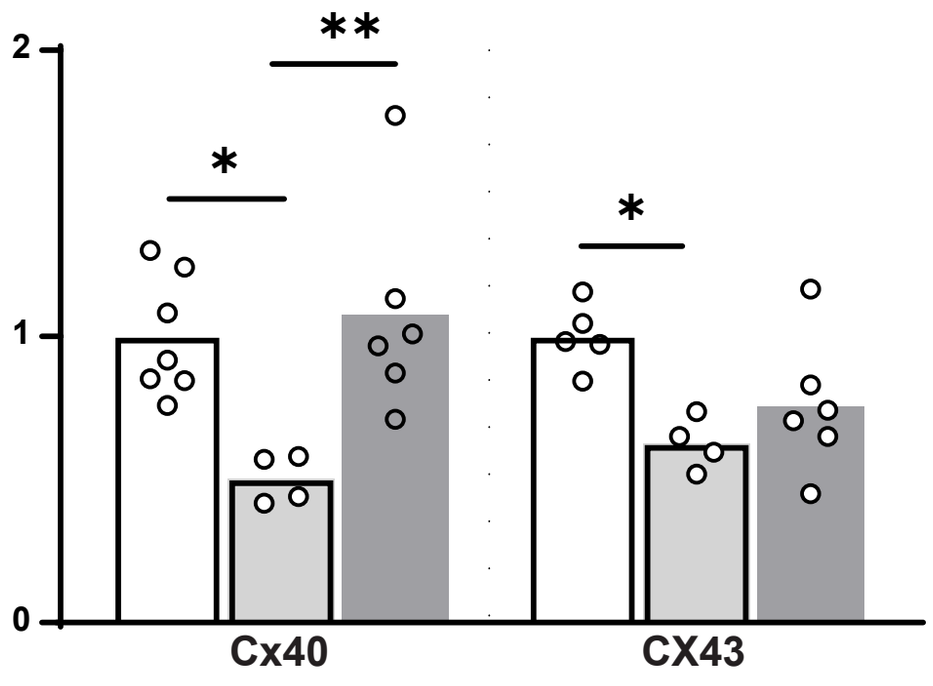

D

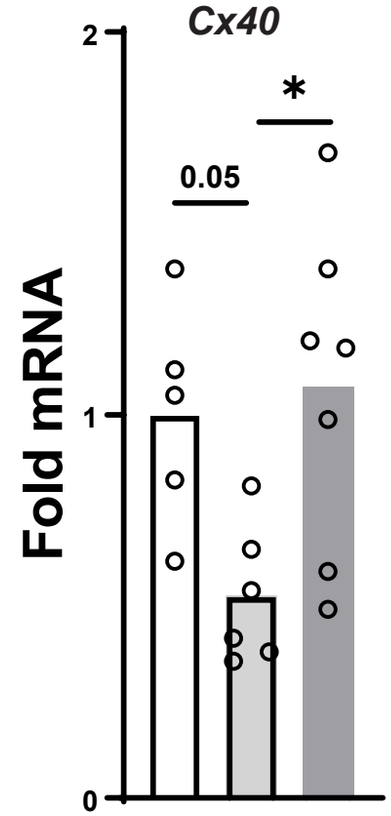

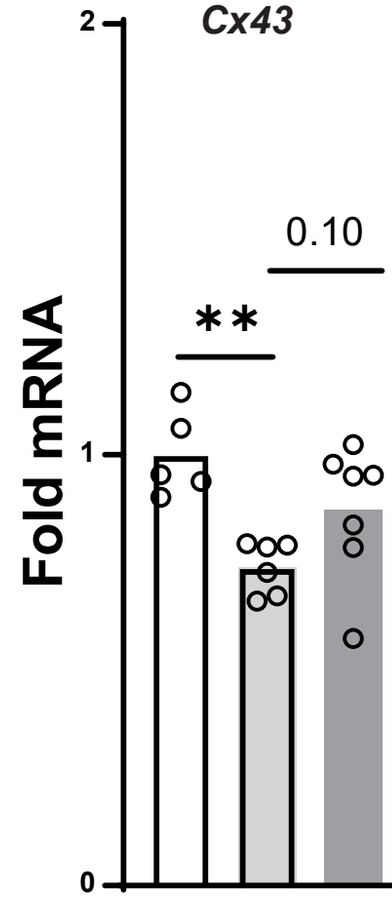

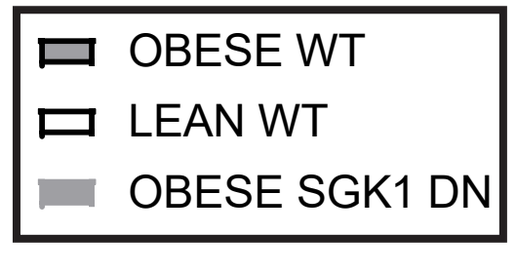

Figure 6: SGK1 genetic inhibition prevents obesity-induced atrial inflammatory signaling. ***A*** Atrial inflammatory gene transcript levels. One-way ANOVA, Dunnett's test. *P<0.05, **P<0.01, ***P<0.001. ***B*** Atrial macrophage content in lean and obese atria as measured by flow cytometry. One-way ANOVA. ***C*** Caspase 1 activity in obese atrial tissue as measured with a commercially available assay. Unpaired student's t-test. *P<0.05. ***D*** Western blots of atrial NLRP3 and caspase subunits with quantification below. One-way ANOVA, Dunnett's test. *P<0.05. ***E*** Western blots of atrial NFKB subunit p65 and its phosphorylated isoform with quantification below. One-way ANOVA, Dunnett's test. *P<0.05, **P<0.01. Number of mice in each group is represented by the number of dots in individual figure.

A

Ccl2

ANOVA p 0.05

Ccl5

Ccl6

Cxcl10

0.12

Vcam1

0.08

Nlrp3

ANOVA p 0.06

IL-1β

Fold mRNA

B

ANOVA p 0.07

Macrophages/mg

C

Caspase 1 Activity (A.U.)

D

NLRP3

110 kD

vinculin

116 kD

Lean WT

Obese WT

Obese SGK1 DN

ProCaspase-1

50 kD

Caspase-1 p20

20 kD

vinculin

116 kD

Lean WT

Obese WT

Obese SGK1 DN

Fold Protein

NLRP3

ProCaspase 1

p20

E

p-p65

65 kD

NFkB p65

65 kD

vinculin

116 kD

Lean WT

Obese WT

Obese SGK1DN

Fold Protein

p-p65

NFκB p65

OBESE WT

LEAN WT

OBESE SGK1 DN

Figure 7: Constitutive SGK1 activation may increase susceptibility to obesity-induced AF. ***A*** Lean SGK1 CA and lean WT littermates were studied with EP studies and optical mapping. ***B*** Inter-atrial difference in APD50 in SGK1 CA atria. Paired Student's t-test. *P<0.05. ***C*** Optical mapping derived action potential duration at 90% repolarization in RA (top) and LA (bottom) with representative AP tracings. Unpaired Student's t-test. *P<0.05. ***D*** SGK1 CA and WT mice were fed a HFD for 6 weeks and then underwent electrophysiologic and biochemical studies. ***E*** Electrophysiologic assessment of WT and SGK1 CA mice fed HFD for 6 weeks with telemetry for PAC quantification (top left) and invasive electrophysiologic studies to determine AF inducibility (>1s) (top right), total AF burden during EP study (bottom left), and total number of AF episodes >250ms (bottom right). P values obtained with unpaired Student's t-test for PAC count, Fisher exact test for AF inducibility, and Mann-Whitney test for AF burden and frequency. *P<0.05. ***F*** Optical mapping derived action potential duration at 90% repolarization in RA (left) and LA (right) with representative AP tracings. Unpaired Student's t-test. *P<0.05. ***G*** qRT-PCR derived expression of *Col1A1* and *NLRP3* atrial tissue. Unpaired Student's t-test. *P<0.05. Number of mice in each group provided in bar graph or represented by the number of dots in individual figure.

A

SGK1 CA
or
WT
6 weeks old

Control
Chow
x 10 weeks

EP Study
Optical Mapping

B

LEAN WT

APD 50% (ms)

14
7
0

ns

RA LA

LEAN SGK1 CA

APD 50% (ms)

14
7
0

*

RA LA

C

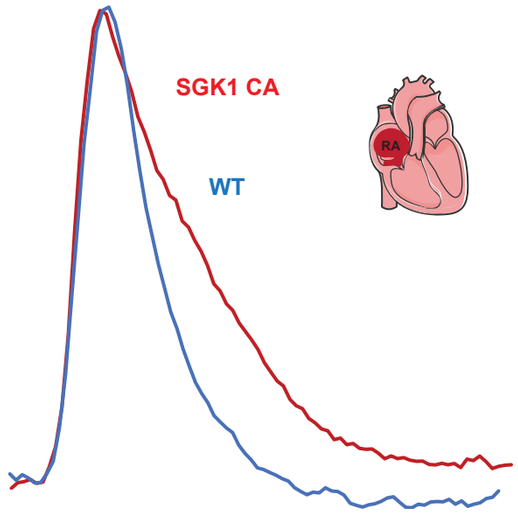

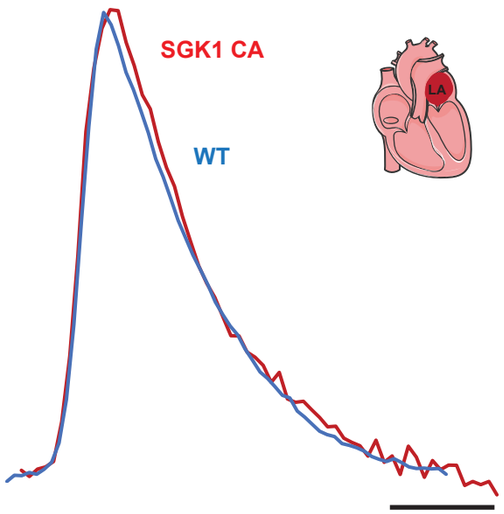

APD 90% (ms)

20
15
10

*

APD 90% (ms)

20
15
10

ns

D

SGK1 CA or WT
6 weeks old

High Fat Diet
x 6 weeks

Telemetry
EP Study
RT-qPCR
Optical Mapping

E

PAC Count (#)

30
15
0

*

% AF Inducibility

100
50
0

10 14

Total Time in AF (s)

600
300
0

0.05

AF Episodes > 250ms

20
10
0

*

G

Col1A1

Fold mRNA

3.0
1.5
0.0

*

Nlrp3

Fold mRNA

3.0
1.5
0.0

*

F

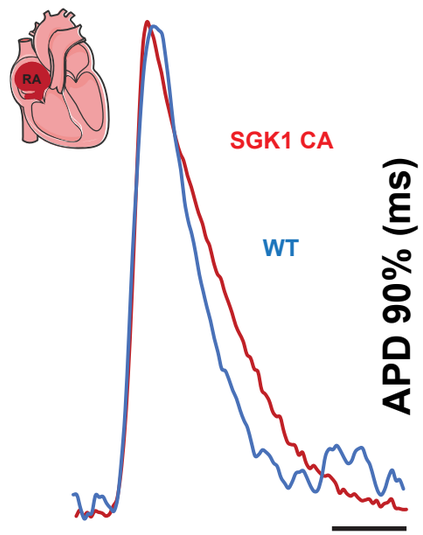

APD 90% (ms)

40
20
0

*

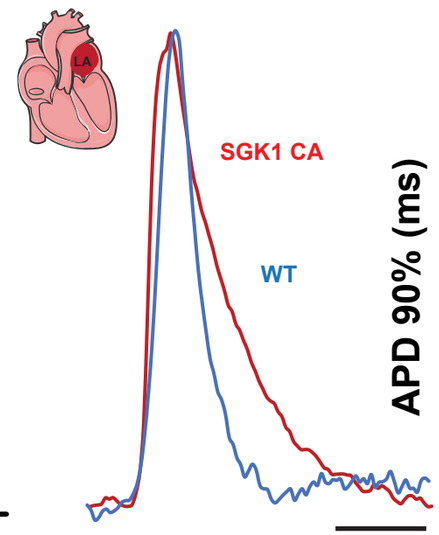

APD 90% (ms)

30
15
0

*

WT SGK1 CA

Tables

Table 1. Upregulated enriched KEGG pathways known to be associated with SGK1 signaling

KEGG Pathway	Size	NES	Nominal p-value	FDR q-value	FWER p-value
KEGG_FOCAL_ADHESION	194	3.56	0	0	0
KEGG_REGULATION_OF_ACTIN_CYTOSKELETON	201	3.14	0	0	0
KEGG_CHEMOKINE_SIGNALING_PATHWAY	166	2.74	0	1.32E-04	0.001
KEGG_JAK_STAT_SIGNALING_PATHWAY	116	2.45	0	0.001533	0.018
KEGG_INSULIN_SIGNALING_PATHWAY	129	2.42	0	0.001611	0.023
KEGG_MAPK_SIGNALING_PATHWAY	252	2.30	0	0.003421	0.058
KEGG_TOLL_LIKE_RECEPTOR_SIGNALING_PATHWAY	87	2.23	0.0039	0.004415	0.082
KEGG_MTOR_SIGNALING_PATHWAY	50	1.73	0.0204	0.051973	0.884
KEGG_B_CELL_RECEPTOR_SIGNALING_PATHWAY	72	1.70	0.0276	0.055648	0.909
KEGG_ALDOSTERONE_REGULATED_SODIUM_REABSORPTION	39	1.47	0.0883	0.138795	1

NES, normalized enrichment score. FDR, false discovery ratio. FWER, family-wise error rate.

Table 2. Cardiac electrophysiological parameters determined with in vivo EP study in lean WT, obese WT, and obese SGK1 DN mice

	LEAN WT (n=3)	OBESE WT (n=9)	OBESE SGK1 DN (n=9)
Basic EKG Parameters			
BCL (ms)	118±18	130±19	126±16
PR_{100ms} (ms)	40±5	47±8	45±7
QRS_{100ms} (ms)	28±3	31±3	29±3
Sinus node function			
$SNRT_{80ms}$ (ms)	135±10	169±28	167±65
AV node characteristics			
Wenckebach cycle length (ms)	73±6	75±5	76±5
Atrial characteristics			
$AERP_{100ms}$ (ms)	24±7	31±5	30±6
Ventricular characteristics			
$VERP_{100ms}$ (ms)	29±7	30±5	32±7
Atrial Arrhythmias			
Inducibility (%)	0*	100	22*
Burden (s)	0.8±1.5*	91±138	1.5±3*
Frequency (#)	1.3±2.3	6±5	1.6±3*

Data are mean±SD; asterisk (*) indicates $P<0.05$ compared to obese WT. Fisher-exact testing for AF inducibility. Kruskal-Wallis with post-hoc Dunn's test for AF burden/frequency. Subscript denotes PCL where appropriate. BCL, basic cycle length; PR_{100ms}, PR interval duration; QRS_{100ms}, QRS duration; SNRT, sinus node recovery time; $AERP_{100ms}$, atrial effective refractory period; $VERP_{100ms}$, ventricular effective refractory period.

Table 3. Optical mapping derived action potential durations, conduction velocity, and AP upstroke velocity in WT and SGK1 DN atria

	LEAN WT	OBESE WT	OBESE SGK1 DN
Right Atrium	**N=7**	**N=15**	**N=19**
CV (m/s)	0.61±0.20	0.67±0.26	0.61±0.14
APD50 (ms)	10.9±2.0	11.1±1.2	10.0±1.7
APD70 (ms)	17.7±2.9	17.9±2.1	16.1±2.6
APD90 (ms)	21.6±2.9	21.7±2.7	19.6±2.7*
dV/dt (%/ms)	27.8±6.7	29.1±4.4	30.5±5.3
Left Atrium	**N=7**	**N=11**	**N=15**
CV (m/s)	0.69±0.17	0.78±0.32	0.74±0.22
APD50 (ms)	10.9±4.2	9.4±1.3	8.9±1.7
APD70 (ms)	18.6±7.4	15.9±2.7	14.6±2.6
APD90 (ms)	22.4±7.5	20.9±2.5	18.0±2.9*
dV/dt (%/ms)	34.5±3.7	34.4±3.6	31.4±4.3

Data are mean±SD; asterisk (*) indicates $P<0.05$ compared to obese WT. One-Way ANOVA, Dunnett's test. PCL 100ms for all measurements. CV, conduction velocity; APD50, action potential duration at 50% repolarization; APD90, action potential duration at 90% repolarization; dV/dt, AP upstroke velocity from 20-80% depolarization calculated as percent per ms.